Summer November 2014

PATTERNING AND MECHANICAL ANALYSIS OF FIBER-BASED MATERIALS

Samuel A. Pendergraph
University of Massachusetts Amherst

PATTERNING AND MECHANICAL ANALYSIS OF FIBER-BASED MATERIALS

A Dissertation Presented

by

SAMUEL PENDERGRAPH

Submitted to the Graduate School of the
University of Massachusetts in partial fulfillment
of the requirements for the degree of

DOCTOR OF PHILOSOPHY

September 2014

Polymer Science and Engineering

PATTERNING AND MECHANICAL ANALYSIS OF FIBER-BASED MATERIALS

A Dissertation Presented

by

SAMUEL PENDERGRAPH

Approved as to style and content by:

_____
Kenneth R. Carter, Co-Chair

_____
Alfred J. Crosby, Co-Chair

_____
Julie M. Goddard, Member

_____
David A. Hoagland, Department Head
Polymer Science and Engineering

ACKNOWLEDGMENTS

I would like to first and foremost thank my advisors Prof. Kenneth R. Carter and Prof. Alfred J. Crosby. The guidance I have received allowed me to not only gain the insight and knowledge I sought when I entered graduate school, but it greatly exceeded those expectations. More importantly, I learned new ways on how to view and approach problems. Under their guidance, I discovered new passions in research that I will carry with me for the rest of my life. Through their support and tutelage I was able to complete my graduate studies and foster my growth not only as a researcher but as person. I am forever in debt to my mentors.

I would also like to thank my other committee member, Prof. Julie M. Goddard. The insight I gained on scientific presentations skills, data analysis, and approaching problems was invaluable for my thesis and development as a scientist. I would like to thank the faculty of Polymer Science and Engineering for also fueling the desire to continue to study the field. The courses were exceptional and always an inspiration to my studies. I would also like to thank the staff of PSE, without you I would be hopelessly lost. Thank you for being helpful and friendly people.

I want to thank all of my friends I have met in my time at PSE. Particularly, I would like to thank the entering class of 2007 and my lab mates in both the Carter and Crosby research groups. You will never just be my colleagues; you are some of my closest friends. It has been the best time to share this experience with all of you. Most importantly, I would like to thank my friends at 24 Summer Street. It was truly a time of

my life I will never forget and I would never want to spend my graduate school years any other way.

Finally, I would like to thank my family and friends. Without their love and support, this thesis would not be possible. I dedicate this thesis to my family as a gesture of my gratitude. I love you all.

ABSTRACT

PATTERNING AND MECHANICAL ANALYSIS OF FIBER-BASED MATERIALS

SEPTEMBER 2014

SAMUEL PENDERGRAPH, B.S. UNIVERSITY OF CONNECTICUT

M.S. UNIVERSITY OF MASSACHUSETTS,

Ph.D. UNIVERSITY OF MASSACHUSETTS

Directed by: Kenneth R. Carter and Alfred J. Crosby

The ability to define and control the topography of a surface has been studied extensively due to its importance in a wide variety of applications. The control of a non-planar topography would be very valuable since a number of structures that are pervasive in artificial applications (e.g. fibers, lenses) are curved interfaces. This potential of enabling applications that incorporate non-planar geometries was the motivation for this thesis. The first study of this thesis comprises the study of patterning the circumference of micrometer sized fibers. Specifically, a unique technique was described to pattern the fiber with a periodic array of colloids. The effect of immobilizing fibers on different substrates and the parameters that govern a successful transfer of the colloidal array onto 7 μm diameter fibers were studied. Finally, replication of inverse submicrometer patterns onto the diameter of the fiber is completed with mild removal of the colloidal template.

The second component of the thesis is the patterning of fabric assemblies of fibers. Composites of soft elastomer resins and rigid fiber materials are explored for their complimentary properties. Specifically, the organization of the fiber structure was

contrasted with other homogenous materials. These composites were shown to possesses rigid in-plane strength, yet remain flexible to bending deformation. Furthermore, the carbon fiber fabric composites demonstrate superior tensile strength and greater flexibility than common homogenous materials such as PET and cross-linked elastomers. Finally, the use of a liquid resin permits submicrometer patterns to form on the periphery of the fabric assembly.

The final component of the thesis is the use of the patterned fabric assemblies for adhesive applications. Carbon fiber-elastomer composites were patterned with submicrometer shear adhesion. The effects of the pattern size and orientation on the shear adhesion were studied. By varying the velocity of the sample testing, adhesion was observed to change for different patterned samples. We highlight the aspects of the fabric composite and the patterning that permits the features to alter the adhesion. Finally, we suggest how these results could be designed to improve the shear adhesion of reversible adhesives.

TABLE OF CONTENTS

Page

LIST OF FIGURES

CHAPTER 1

INTRODUCTION

1.1 Project Overview

A material's surface topography can have a great influence on the behavior in its given environment. This has been observed in copious examples found in nature where organisms utilize special topographical features as an adaptive means to survive. For instance the surface of a lotus leaf has a hierarchical structure to repel water as a self-cleaning mechanism.[1, 2] The Tokay Gecko is another example of using complex topographical features to facilitate its ability to adhere and climb up structures. [3-9]

Patterning surfaces has also been explored in artificial systems as a means to control surface interaction. Recent developments in methods such as photolithography have facilitated the growth of the electronics industry.[10-15] Creating small, discrete conductive features has led to the formation of complex circuitry leading to more powerful electronics while reducing the size of the device.[10, 11, 16] Another application where patterning has been particularly fruitful is the use of patterns to create discrete regions for biomedical applications.[17, 18] Control of drug release kinetics and increased sensitivity of diagnostics are two improvements that have been realized through patterning.[17-20] It is apparent that altering the topography of a surface has significant implications on the behavior of an application.

Advances in patterning have led to improvements in many applications. However, many of these studies focus on patterning planar materials. Non-planar substrates are ubiquitous in nature as well as synthetic constructions. However, the patterning of these substrates in synthetic applications is challenging. This thesis

addresses some of these challenges of patterning on non-planar materials. The second chapter is a study on the patterning of individual fibers with a colloidal template and the subsequent use of this template to create uniform patterns on the fiber perimeter. The third chapter is an evaluation of mechanical properties of soft elastomeric-fabric composites and the patterning of these fabric composites. Applying the patterning techniques from chapter 3, the fourth chapter is the study of shear adhesion with the patterned fabric composites. These chapters highlight the ability to control the topography of non-planar interfaces and subsequently demonstrate one application of the patterned surfaces.

1.2 Motivation

Fibers and fabrics are unique materials because of their strong tensile resistance and bending flexibility that is dictated by their geometry. In modifying the materials and the assembly of individual fibers, the mechanical properties can be tuned. These have led to their use from rigid structural applications in cars to soft clothing and biomedical sutures. However, the curvature in fibers and fabrics creates difficulty in patterning these types of materials. In addressing this problem, we demonstrate two new methods to pattern non-planar geometries.

In the first part of the thesis, we discuss the patterning of individual fibers and the parameters that govern the transfer of a colloidal template onto the fibers. The goal of patterning the fibers is to have a method to tune the surface properties of the fibers themselves. The second part of the thesis describes the patterning of a fabric assembly. Through these experiments, we retain the mechanical qualities of a woven fabric, yet impart new topographies by patterning the surface. In combining these two aspects, we

provide new methods to change the surface properties of fibers and woven fabric assemblies. The final section is the application of the patterned woven fabric assembly and how it can be used to affect adhesion.

1.3 Patterning Materials

Creating patterns on materials has been studied for decades as a means to modify the topography of a surface. Typically, patterning is introduced in order to create high number of discretized features. Arrays of discrete structures on a surface enables the possibility of enabling combinatorial sampling to occur on a single substrate.[21] Another application in creating these arrays is for memory storage and displays. [11, 22] High density arrays of patterns with long range periodic order can also be used for selective and tunable transmission of electromagnetic radiation. [23, 24] Improvements in biomedical diagnostics and electronics have also emerged from advancement of patterning substrates. [11, 13, 15, 17, 20, 25-29] In adhesion applications, the implementation of discrete structures can lead to enhanced adhesion because of the ability of the discrete features to arrest crack propagation.

The implementation of patterning is widely studied on planar substrates, however work on non-planar materials is not is extensive. In nature, non-planar, structured interfaces are commonly observed to facilitate organism adaptability to an environment. The Tokay gecko has an intricate topography on the surface of its feet, which has drastic implications on wettability, adhesive, and sensory attributes of an organism, shown in figure 1.1.[30]

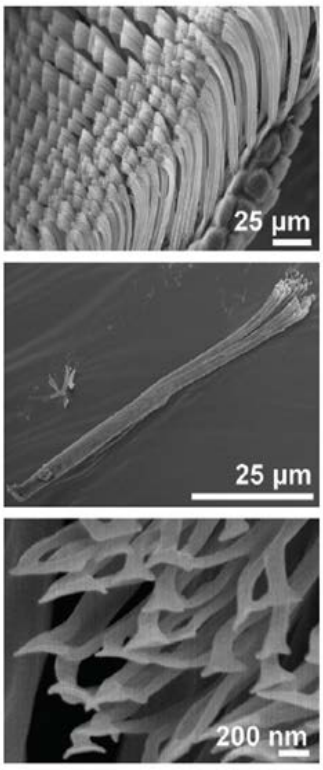

Figure 1.1: Scanning electron microscope (SEM) images of Tokay Gecko's toe. Figure reproduced from literature. [30]

Observations like these from nature have been translated into artificial analogs of these applications. However, as mentioned earlier, these have been used on flat surfaces, which is not representative of the organism. In order to examine the details of patterning non-planar materials, we will review through two widely used patterning techniques.

1.4 Colloidal Lithography

Colloidal lithography has emerged over the last several decades as new method to pattern materials.[21, 23, 31-35] Use of this technique has increased due to new and faster techniques to form colloidal crystal arrays on various substrates.[23, 31, 32, 36] A colloidal crystal serves as a template for patterning, where the colloids occlude regions of a surface from deposition of a material, such as inorganic or polymeric materials[24, 33], shown in figure 1.2.

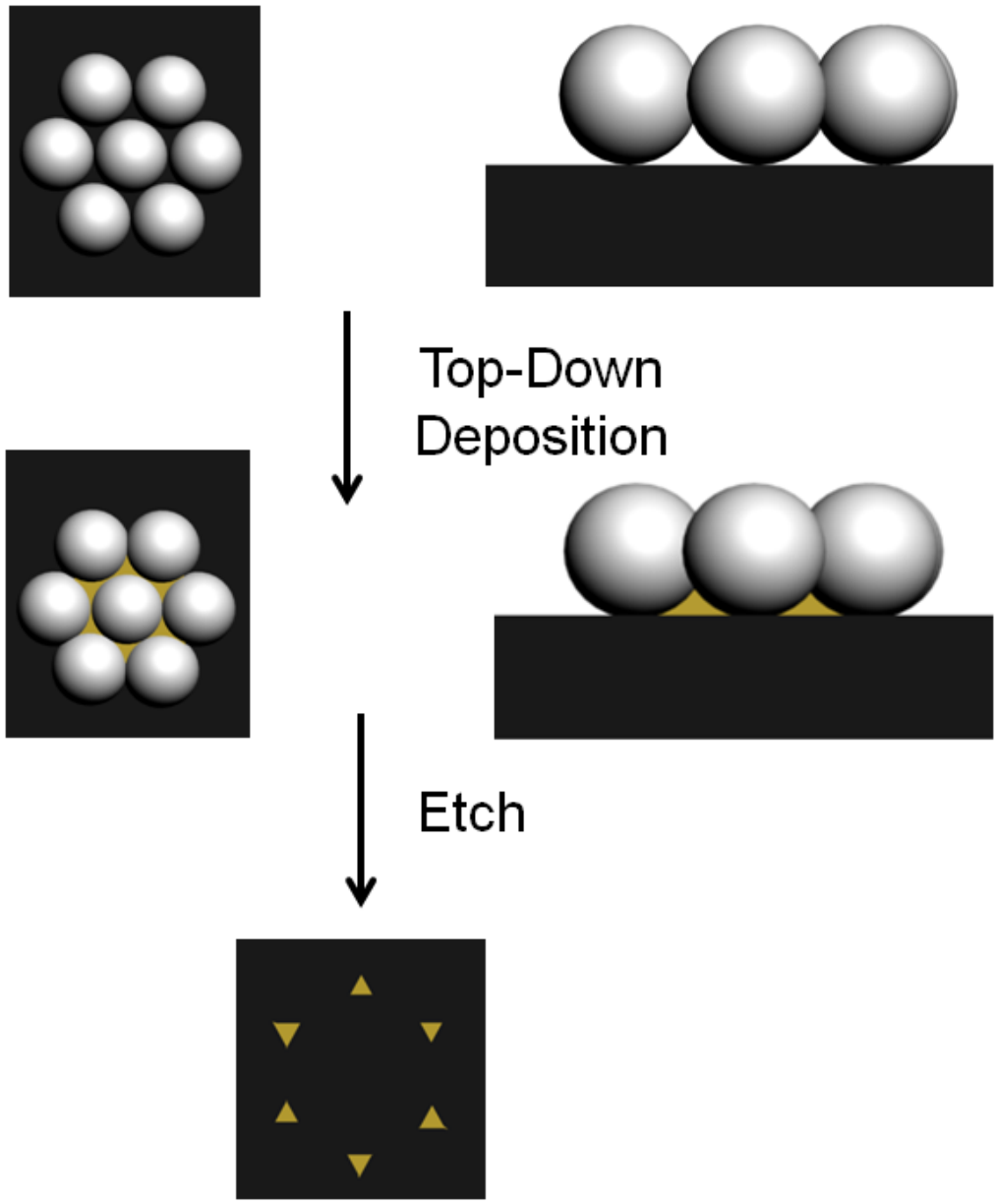

Figure 1.2: Top-down deposition of material into a colloidal template. The second pattern is the subsequent etching step to yield the resulting pattern.

Afterwards, the template is selectively etched away, to leave the patterned deposited material behind. This has been demonstrated as an effective method to create well-ordered, periodic structures. The periodicity and size of the features can be tuned through the packing arrangements of the colloids and variation of the colloidal size. For a hexagonal array of colloidal particles, the width of the patterned feature can be found to

be 0.155 *D*, where *D* is the diameter of the colloidal particle.[24, 33] The distance between adjacent features can also be geometrically predicted as 0.577 *D*, shown in figure 1.2.[24, 33]

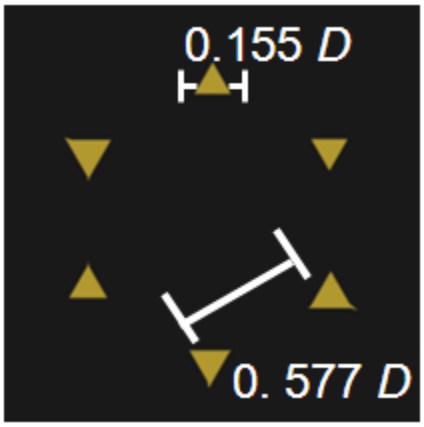

Figure 1.3: Geometric dimensions of top-down colloidal patterning. The resulting pattern from a top-down deposition through a colloidal mask.

Since the diameter of the particle can be adjusted, the spacing and areal coverage of a surface can be tuned. If an evaporative top down process is used (e.g. metal deposition) and the colloidal array is densely packed, discrete patterns will form. This has been demonstrated in previous literature to create inorganic structured surfaces through the evaporation of metal.[21, 33, 35] The aspect ratio of these patterns can be further modified by using the patterned surface as a "seeding" component where more metal is grown off the pattern, leading to the fabrication of higher surface area patterned structures.[37] Finally, by overlapping templates on top of each other, intricate and hierarchical patterns can be formed with colloidal lithography that would be difficult to produce with other patterning techniques. [24, 38]

When the material deposition occurs from underneath the template, and the reagents are allowed to pervade into the interstitial spacing of the colloidal array, a continuous

network can be formed (figure 1.4). [39, 40] The pattern starts from a monomer and is polymerized into a larger structure.

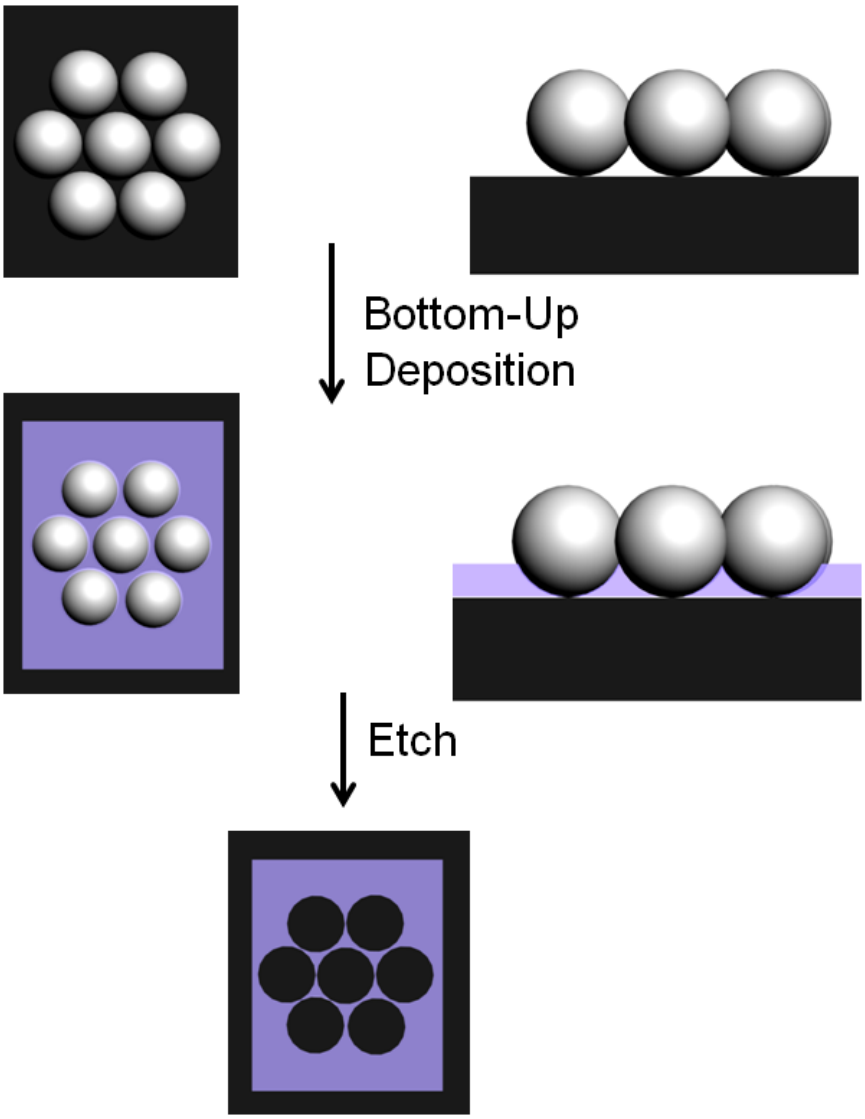

Figure 1.4: Bottom-up deposition of material between a colloidal array. The subsequent pattern is formed after etching.

Inorganic and organic examples have been demonstrated through this patterning technique through electrochemistry as well as solution processing at an air/water interface. Continuous structures can be fabricated in the form of a three dimensional structure. If there is ordering of a colloidal array in three dimensions, rather than a two-

dimensional monolayer, the interstitial spacing can be filled as in the aforementioned case.[24, 41] When the template is removed, an ordered porous structure is created. Colloidal lithography possesses a unique capacity to create nanometer structures that are either discretely located from each other or form a continuous structure with periodic voids. The dimensions of these patterns can easily be adjusted by changing the packing geometry of the array of particles and the colloidal diameter. Both inorganic and organic structures can be fabricated since several etching techniques can be used for template removal. In the scope of the thesis, this patterning method is pertinent due to the fact it has been demonstrated to pattern fibers as well as hemispherical caps easily and with high ordering.

1.5 Imprint Lithography

Imprint lithography is another patterning technique that has garnered attraction in the last 15 years through the advances on the resolution of sizes that can be transferred.[11, 14, 16, 42, 43] The advantages that this technique possesses include the ability for materials to be patterned rapidly and with less cost compared to other nanopatterning methods. The process of patterning involves a film to be patterned and a master mold. In some examples, the film is a low viscosity liquid that when in contact with the master mold will flow into the pattern.[16, 44, 45] After applying a stimulation to the liquid, (e.g. heat, ultraviolet light), crosslinking can occur and a solid network is formed. When the reactions are run to completion, the mold can be removed and a patterned film remains. Intricate and tunable geometries can be easily produced through this method. One drawback of imprint lithography is that, an etching step is required in order to eliminate the residual layer and isolate discrete structures, shown in figure 1.5.

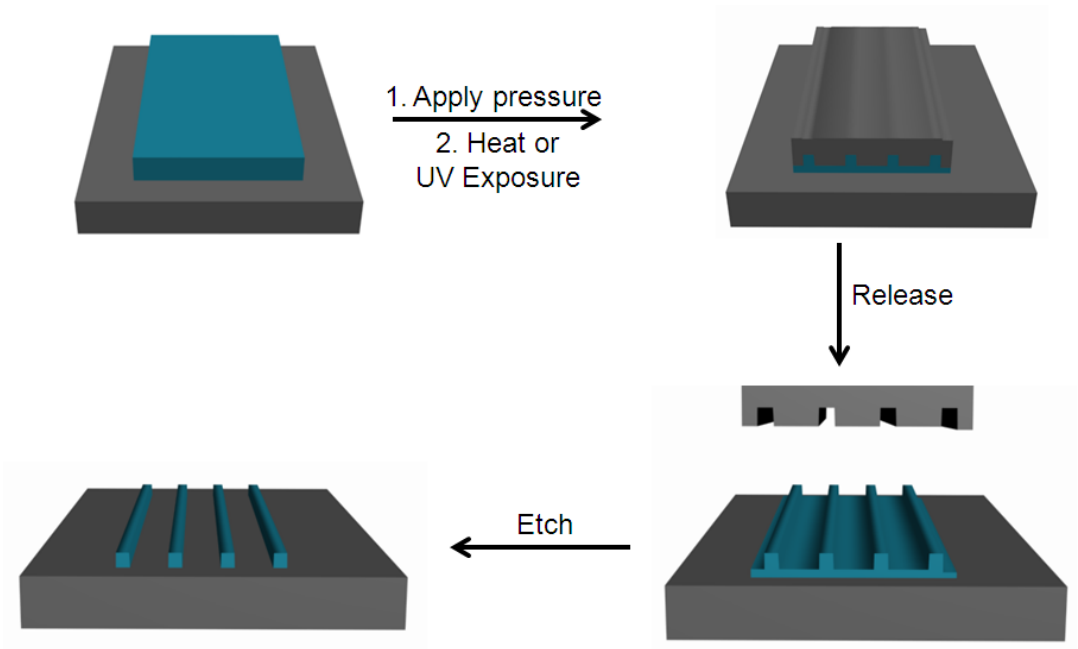

Figure 1.5: Imprint lithography schematic. The imprint lithography technique can provide discrete patterns on a substrate.

The imprint material is not limited to low viscosity liquid precursors, but rigid, uncrosslinked films may also be used. Specifically, the processing requires applying temperature above the glass transition temperature (T_g) or in some cases the melting temperature (T_m) of the polymer. To maintain fidelity in the pattern transfer, it is ideal to use a rigid mold to avoid deforming the master pattern. Upon application of pressure and heat, the film will flow into the mold and conform to the patterns. After cooling the sample down, the film will harden (via crystallization or vitrification) and the mold can be released leaving a patterned film. Similar to patterning with a non-viscous liquid, an etching step is required in order to isolate discrete patterns. However, similar to patterning with colloidal lithography, there is an ability to create a continuous pattern shown in figure 1.6.

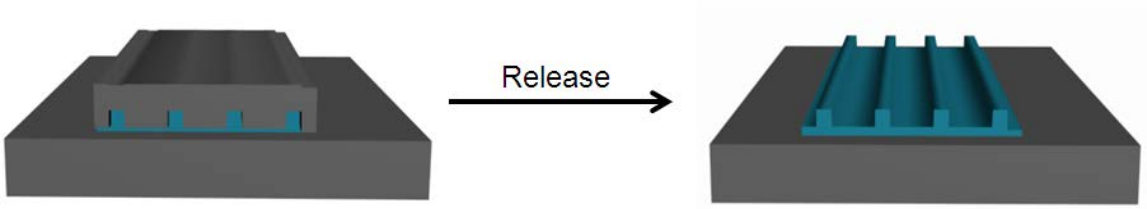

Figure 1.6: Imprinted film with residual layer. The residual layer creates a higher surface area patterned film

The use of high surface area topography is advantageous applications such as catalysis and drug delivery where the exposure of the surface to the environment is required for reactions or transport of material to occur. Another application where high surface area patterns are used is in modifying the adhesion of a surface. For adhesion applications, it is important for the features to act independently; however, the area of contact has to be maximized.

1.6 Patterned Adhesion

In the previous sections, artificial methods for patterning and their applications were discussed. However, complex patterns are observed in nature, which allow an organism adapt to their environment. For example, the Tokay Gecko has evolved a complex, hierarchical structure in order to adhere to a number of surfaces and be able to climb. This has prompted studies to fabricate artificial topographical features and subsequently test the adhesion.[5-8, 30, 46] Researchers have studied the effect of the aspect ratios of the topographical features as well as the frictional forces that are associated with these geometries. While replicas similar to the topography of a gecko have been established, these geometries do not necessarily lead to higher adhesive forces.

Recently, Bartlett *et al.*, has described a scaling relationship for reversible adhesives.[30]

$$F_c \sim \sqrt{G_c}\sqrt{\frac{A}{C}} \tag{1.1}$$

Where F_c is the critical force to detach a sample in shear, *A* is the area of contact and *C* is the total compliance of the system. The compliance of the system is dictated by the most compliant feature of the system being observed. It is apparent from equation 1.1 that maximizing the critical force, for a given area and material system, the compliance of the system must be reduced. In another study, Bartlett *et al.* evaluated the effect the scaling of compliance with pattern aspect ratio.[47] From these results, it has been demonstrated that lower aspect ratio blocks maintain a lower compliance than longer fibrillar structures, given a constant materials system.[47] One way to improve these fibrillar structures is to alter the orientation in order to create a lower compliance. Researchers have demonstrated that creating angled features, similar to the Tokay Gecko, creates a reduction in the system compliance and thus leads to high pull-off stresses.

Adhesion is enhanced when the stiffness is greater, however this is predicated on the ability for features to be brought into contact with the surface. A length scale (a^*) where adhesive forces become important can be estimated by the following relationship:

$$a^* = \frac{G_c}{E} \tag{1.2}$$

Where Gc is the critical energy release rate and E is the elastic modulus of the material. From equation 1.2, it is apparent that the material can conform to larger roughness if the surface interactions (Gc) are more attractive or if the modulus of the material is lower. In the former variable, there is little variability that can be obtained through material modification. Reduction in the modulus will lead to a higher compliance and thus a lower critical force will be realized. Thus there is a balance that must be made between allowing the patterned features to be attached to the surface effectively and possessing strong mechanical stiffness.

1.7 Thesis Organization

The second chapter describes the use of colloidal lithography to pattern microscopic carbon fibers with submicrometer and nanometer sized features. In particular, we discuss the formation of a colloidal array on an air/water interface and the important parameters that dictate the transfer of the colloidal array on the fiber. The role of immobilizing the fiber and the use of various substrates to collect the colloidal films is discussed. Finally, the use of the colloidal array as a dissolvable template for conductive polymers is shown.

The third chapter will describe the fabrication of patterned fabric composites. First, we will describe the one-step process of creating and patterning a bendable elastomeric fabric composite from imprint lithography. The stability of the patterned substrates is demonstrated through a rapid cyclic mechanical testing. The mechanical properties of these fabric composites are shown and compared to demonstrate the unique capabilities of implementing a fabric structure. Finally, an improved ability to create highly tensile load resistant materials while maintaining flexibility is demonstrated.

Finally, in the fourth chapter, materials described in chapter three are applied towards reversible adhesive applications. Patterned elastomeric fabric composites are tested for shear adhesion. The effect of the resin material properties is discussed in relationship to the pattern dimensions. The orientation of the line patterns is tested and discussed. Finally, adhesion enhancement can be demonstrated over non-patterned interfaces.

CHAPTER 2

PATTERNING NON-PLANAR SUBSTRATES WITH COLLOIDAL DRAPING

2.1 Introduction

Patterning materials on the submicrometer and nanometer scale has led to enabling new applications as well as significant improvements of well-developed devices. While patterning has been well studied and developed for decades, the majority of the work has been focused on planar materials or those with a radius of curvature much larger than any dimension of the patterns being formed. In this chapter we will examine the patterning of single micrometer sized fibers with submicrometer and nanometer sized patterns. In this chapter in we will use colloidal lithography as the method to pattern the fibers. In using an assembled, free-standing colloidal array, rather than a suspension of free colloids, a micrometer sized fiber can be decorated with a pattern template. The colloids then serve to block material from being transferred to the circumference of the fiber (i.e. inhibiting electrochemical reactions). This template can easily be removed after the electrochemical patterning.

In this chapter, we address several questions pertaining to the patterning of micrometer sized fibers. First, what are the necessary conditions for successful colloidal array transfer to a fiber surface? Second, how does the colloidal array conform to the circumference of the fiber and what is the consequence of the colloidal packing on the pattern transfer? Finally, what are the conditions for pattern transfer on the fiber surface with the colloidal template in place? Through these questions, a novel procedure was

developed to create reproducible patterns on size scales that previously have not been described with little surface modification or time consuming patterning techniques.

2.2 Background

Patterning on non-planar substrates remains challenging in nanotechnology. In addressing this problem, several methods have been pursued such as soft lithography[43, 48, 49], electron-beam lithography[50, 51], printing[52-54] , wrinkling[55-57] and colloidal lithography.[24, 29, 31, 32, 58-61] The majority of these studies have focused on the patterning of cylindrical fibers, typically smooth optical fibers, which have been limited to a diameter around 0.1 mm.[59, 62-65] One method to patterning such fibers was presented by Whitesides and co-workers with the use of free standing epoxy thin films containing nanoscale metallic features.[66, 67] In their technique, the epoxy matrix is floated on a water surface and an optical fiber is brought into contact with the matrix by pushing the fiber into the water bath. Subsequently, the matrix stretches around the curved surface and the epoxy is subsequently etched in order to complete the patterning with nano-sized metallic features.[66, 67] Although this method is versatile for inorganic structures, the requirement of an oxygen/plasma etch to remove the epoxy material prohibits the patterning of organic materials.

An alternative approach to creating a periodic pattern on a non-planar substrate is through the use of colloidal lithography. The majority of previously described methods using colloidal templates have focused on the crystallization of dispersed colloids on the surface of an optical fiber through a dip-coating method or a controlled evaporation technique.[23, 36, 65, 68] Recently, Jia and co-workers have published several papers on the coating of flat and curved interfaces with a non-densely packed colloidal array trapped on

an air-water interface through a contact transfer process.[58, 69] The substrate was brought into contact with the film while pushing the substrate into the water. Chemical modification from a hydrophilic to a hydrophobic silicon wafer was required to maintain the order in the colloidal film after the transfer process. Without this surface treatment, the film was disrupted due to strong capillary forces upon removal from the water bath.[58, 69, 70] Furthermore, for patterning non-planar substrates with this approach, an extra polymer layer was required to increase adhesion of the particles to the surface which occludes the desired patterning surface from certain subsequent patterning techniques (e.g. electrochemistry).

In the study presented here, we describe a new and simple method to collect polystyrene (PS) colloidal array films on an air-water interface and deposit them onto rough, carbon fibers that are supported on various substrates on centimeter length scales. We implement carbon fibers to demonstrate the capability of colloidal draping on fibers several orders of magnitude smaller than optical fibers, without chemical modification to any components. Furthermore, by using a conductive carbon fiber, the PS colloidal array was then used as a lithographic template for electrochemical polymerization of poly(3,4-diethoxy thiophene)/poly(styrene sulfonate) (PEDOT/PSS), enabling the ability to pattern well-ordered, submicrometer (< 300 nm) features directly on a rough 7 μm fiber.

2.3 Experimental

2.3.1 Materials

Polystyrene latex beads (200 nm and 500 nm in diameter, 2.5% solids (w/v) aqueous suspension) and poly(styrenesulfonate) sodium salt (PSS, M_w = 70,000 g/mol) were purchased from Alfa Aesar Corp. 3,4-ethylenedioxythiophene (EDOT) were

purchased from Aldrich (Milwaukee, WI). Sodium dodecyl sulfate (SDS) was purchased from Fisher Scientific. Dow Corning Sylgard™ 184 PDMS was purchased from Dow Corning (Midland, MI). Carbon fibers (1k) were purchased from Composite Envisions (Wausau, WI). All reagents and materials were used without further modification.

2.3.2 Formation of the Immobilized Carbon Fibers

First, Dow Corning Sylgard™ 184 base and crosslinking agent were mixed together at a 10:1 ratio, respectively (which will be referred to as x-PDMS). After degassing, the mixture was poured into a petri dish and precured for 20 minutes at 70^{o}C. Fibers were then individually separated from a bundle of carbon fiber and placed on top of the precured x-PDMS.[71] The x-PDMS was then completely cured for another 2 hours at 70^{o}C.

2.3.3 Formation of Colloidal Array Template

Glass slides were cleaned with deionized (DI) water and sonicated for 10 minutes at room temperature. Next, the slides were dried under a stream of N_2 gas and placed for ultra violet ozone (UVO) treatment for 10 minutes. After the treatments, 80 μL of the PS colloidal solution was spread over the entire area of the clean glass slide, and the colloids were then spin-coated at 750 rpm for the 500 nm colloids and 1000 rpm for 200 nm colloids for 3 minutes. Immediately after spin-coating, the samples were floated on a water bath. Afterwards, 300 μL of a 2 wt% solution of SDS was spread onto the water surface to create a more densely packed floating PS colloid film.[71]

2.3.4 Transfer of the Colloidal Array to the Immobilized Fibers

After the Sylgard 184 substrate with fibers was submerged underneath the colloidal film, it was manually raised so that the PS film in solid state draped over the

substrate, with a thin layer of water entrained between the colloids and the substrate. In order to quantify the critical velocity with an automated stage, the substrate was withdrawn at a constant velocity of 10 μm/sec and 1 mm/sec to evaluate the effect of coating with velocity using an Exfo Burleigh Inchworm Nanopositioner. After the film was collected, any excess water was drained away slowly by applying a paper towel to the edge of the film. Finally, the substrate containing the film was allowed to dry for 24 hours at room temperature under ambient conditions.[71]

2.3.5 Formation of Inverse Colloidal Array Template via Electrochemistry

The electrochemical synthesis was carried out in a three-electrode cell using a potentiostat (Epsilon, BASi Co.) to electropolymerize PEDOT:PSS film on carbon fibers. The working electrodes was the PS colloid array covered carbon fibers. A platinum wire and an Ag/AgCl electrode were used as counter and reference electrode, respectively. An aqueous solution of 0.01 M EDOT and 0.1104 g (7.89×10^{-5} M) PSS was prepared. A constant potential (potentiostatic method) of 0.9 V vs. Ag/AgCl was applied on the working electrode for 900 seconds. After electropolymerization, the working electrode was carefully rinsed with DI water and then dried overnight. Toluene was used to remove the colloidal template on the fibers.

2.3.6 Characterization

SEM images (FEI Magellan FESEM or JEOL Omniscope) were taken to investigate the surface features of the carbon fibers, colloidal patterned fibers and porous PEDOT:PSS film on the fibers. Optical profilometry was performed on a Zygo New View 7300. An individual fiber was separated from the bundle and taped down to a glass slide. The optical profilometry measurement was run using a 50x objective. The carbon

fiber was found to have a RMS roughness of 150 nm and a maximum valley-to-peak roughness of 660 nm, measuring along the length of the fiber. Contact angle measurements were taken on a VCA Optima from AST Products Inc. Contact angle measurements were then made on the on the PDMS substrate with fibers to measure the contact angle, 118.2˚ +/- 1.4˚ advancing and 82.38˚+/- 6.6˚ receding. Contact mechanic measurements for the modulus of the partially cured PDMS were performed on a custom built instrument. A glass cylindrical probe (r=2.5 mm) is brought into contact with the partially cured PDMS after cooling down to room temperature. The displacement and force were measured using a custom made LabView program. The displacement was controlled with an Exfo Burleigh Inchworm Nanopositioner. The contact area during the testing was measured with a CCD camera (Pixelfly) that was attached to a microscope (Zeiss Axiovert 200M). The sample was pushed into the sample to a maximum load of 2 mN and then the probe was held at that displacement and the stress was allowed to relax for 300 seconds (see supplemental information for derivation of stress relaxation). The relaxation time was found using a Maxwell model described elsewhere.[72] Image analysis of the inverse template features was performed using Image J software.[73]

2.4 Results and Discussion

2.4.1 Effect of Substrate on Coating Process

PS colloidal arrays were prepared by spin-coating an aqueous solution of 2.5 wt% PS colloidal solution on a cleaned glass slide. A schematic of the coating process is shown below in figure 2.1[71]:

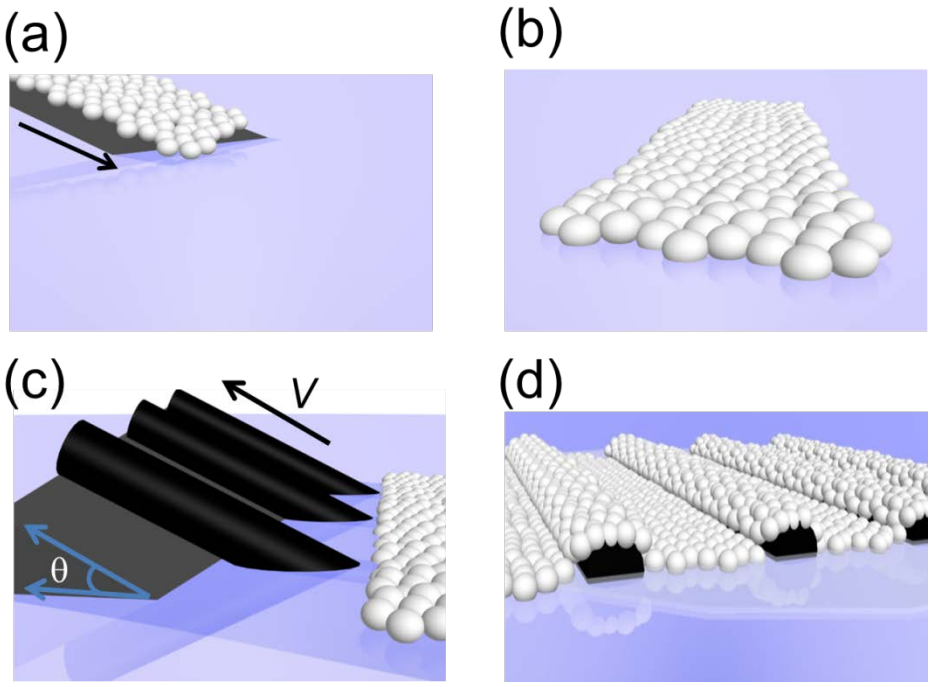

Figure 2.1: Transfer process of colloids onto carbon fiber. A) Transfer of the PS colloidal array from a glass substrate to the air/water interface; B) PS colloidal array resting on the air/water interface; C) A substrate containing immobilized carbon fibers is withdraw from underneath at a given velocity and angle; D) The PS colloidal film wrapping around the fibers as the thin supporting layer of water is evaporating. Figure reproduced from Pendergraph *et al.*[71]

Immediately after the PS film was formed on the glass slide, the array was floated on a water bath containing sodium dodecyl sulfate (SDS). Delay in floating the film led to strong adsorption of the colloids onto the glass slide and created difficulties in the transfer to the air/water interface. The charges on the PS colloids and the SDS provide strong capillary cohesion and resistance to in-plane deformations for the colloids.[70] A substrate supporting carbon fibers was then submerged below the air/water interface and was withdrawn from the water bath to collect the film. The transfer of the film by withdrawing from the water bath was critical in enabling the use of both hydrophilic and hydrophobic surfaces, which cannot be accomplished easily by pushing such substrates into the bulk water bath.[69]

The use of a substrate is essential in this coating technique, but we have found that several different substrates can be used to collect the colloidal film at varying velocities (0.01 mm/sec-1mm/sec) without disrupting the periodicity of the film. The supporting substrate can be withdrawn at different angles, ranging from 0-90^{o} , shown in figure 2.2.

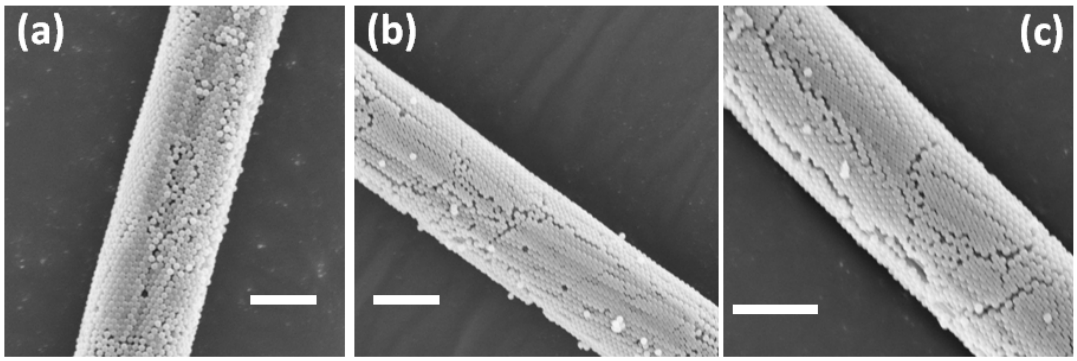

Figure 2.2: Angle dependence of colloid transfer. A) A 500 nm colloid coated carbon fiber after being supported on a hydrophilic glass substrate being pulled at an angle of 15^{o} B) A 500 nm colloid coated carbon fiber after being supported on a hydrophilic glass substrate being pulled at an angle of 45^{o} C) A 500 nm colloid coated carbon fiber after being supported on a hydrophilic glass substrate being pulled at an angle of 90^{o} (All scale bars = 5 μm). Figure reproduced from Pendergraph *et al.*[71]

A necessary condition for this transfer process is that a thin layer of water must be entrained between the surface and the colloidal array. The water supports the colloidal film, and as the water evaporates, the colloidal film wraps around the fiber, creating a conformal contact. Since the colloids are supported on a thin layer of water and not in direct contact with the fiber or the substrate, alignment of the fibers in the transfer process has been found to not be critical. For hydrophilic substrates, the entrainment of water is simply achieved.

Hydrophobic substrates, such as a cross-linked poly(dimethylsiloxane) (x-PDMS), can also be used (Figure 2.3).

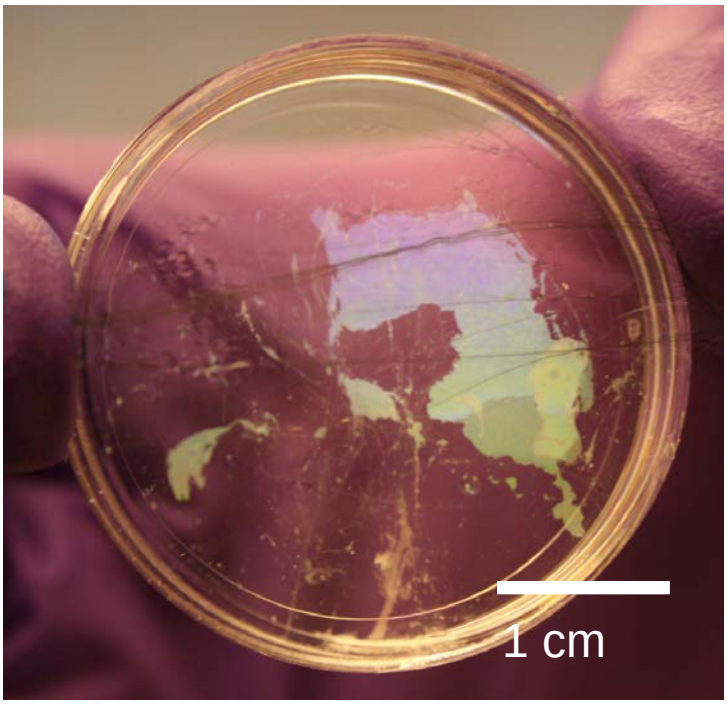

Figure 2.3: A macroscopic picture of a PS colloidal array. The array was collected on a hydrophobic substrate (Sylgard 184). Figure reproduced from Pendergraph *et al.*[71]

However a larger withdrawing velocity is required in order to entrain water between the colloidal film and the substrate. If we use an approximation from previous work[74] for a critical velocity, V_c, needed to lubricate a PDMS substrate this critical velocity is $V_c \approx \gamma \ (1-\cos\theta_e)^3/750\eta$, and where γ is the surface tension (≈0.03 N/m), θ_e is the equilibrium contact angle of the three phase contact line ($1-\cos\theta_e \approx 0.3$) and η is the viscosity of water (≈0.001 Pa•sec).[74] For our conditions, we find a critical velocity of approximately 1 mm/s. This is consistent with the observed velocities required in our fabrication procedure for hydrophobic substrates. Below this critical velocity, water "drains" away from the interface, preventing a continuous layer of water to be formed below the colloidal array. In this case, the colloidal film contacted the PDMS surface and shear forces developed in the colloidal array. This led to undesirable distortion and

fracture within colloidal crystal plane, as the shear force exceeds the cohesive capillary forces holding the colloidal array together.[70] Since the substrate was being pulled out of the water, if this critical velocity was not reached, water will drain away from the interface, preventing a continuous layer of water to be formed below the colloidal array. Film coating does not initiate below this critical velocity. If the critical velocity of the film coating process is attained, then the colloidal film will float on top of the water layer and transfer to the substrate. However, if the withdrawing speed was slowed below the critical velocity, the colloidal film adheres the PDMS surface without a layer of water and shear forces develop in the colloidal array. This leads to undesirable distortion and fracture along the colloidal crystal plane. At this point, the colloidal film fractures and the coating procedure was interrupted due to the film floating away from the air/water/substrate interface.

In general, the PS colloidal array was collected with the substrate tilted at an angle relative to the film on the surface (~ 15^{o}) for our experiments, as shown in Figure 2.2, but a wide range of angles have produced successful patterns.

As mentioned earlier, one important parameter of successful transfer of the array on the substrate is a thin layer of water that supports the colloids. The result after the water is drained from the surface of the fiber, is wrapping of the colloidal array around the fiber, shown in figure 2.4.

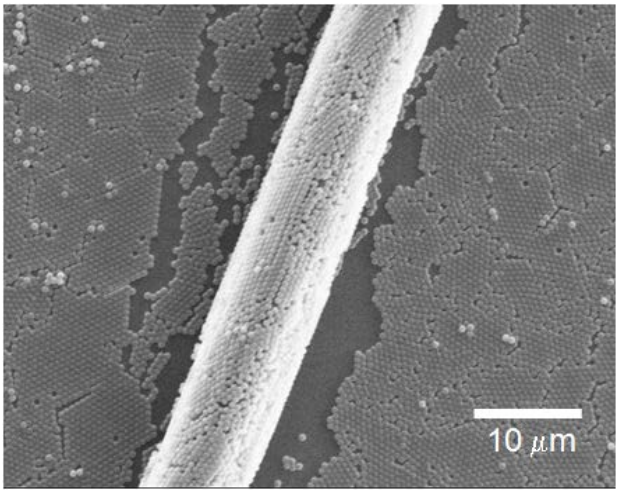

Figure 2.4:SEM image of 500 nm array on fiber and substrate. An array of 500 nm PS colloids transferred to a carbon fiber supported by x-PDMS. Figure reproduced from Pendergraph *et al.* [71]

An interesting aspect of this coating technique is that the transfer process can be used on a non-continuous substrate, such as copper grid, as long as the spacing between solid supporting materials, e.g. grid bars, allows the water film supporting the colloidal array to remain continuous. In our example, a 1mm x1 mm copper mesh was used and the water supported colloidal array was unable to drain through the mesh when collected (Figure 2.5).

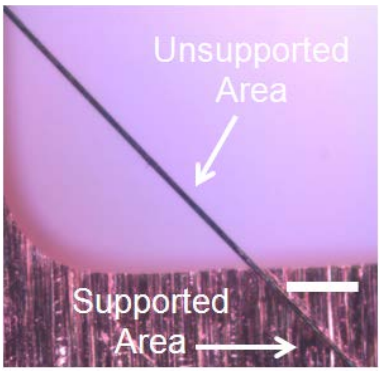

Figure 2.5: Optical microscope image of colloidal array on fiber and copper grid. An optical microscope image after a 500 nm colloidal array was collected on 1mm x 1mm mesh copper grid supporting carbon fibers. Scale bar = 100 μm. Figure reproduced from Pendergraph *et al.* [71]

However, when a large area (2cm x2 cm) was cut out of the mesh, water easily passed through the opening and the fibers acted as a free standing fiber with no supporting substrate. This lack of continuity in the water film led to increased number of defects in the colloidal coating on the fiber (Figure 2.6).

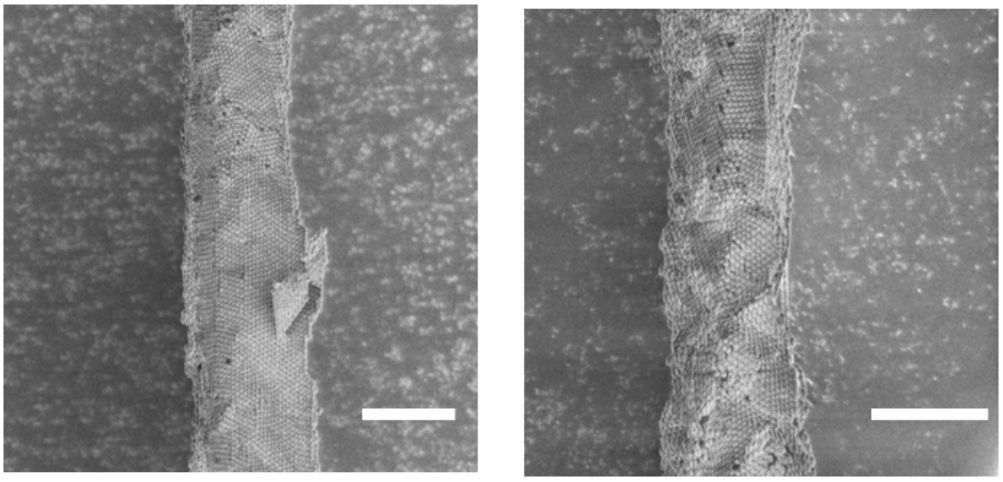

Figure 2.6: Colloidal array collected on free standing fiber. Images of a 500 nm PS colloidal array that was collected on a free standing carbon fiber. Scale bar = 10 μm. Figure reproduced from Pendergraph *et al.* [71]

If we observe the unsupported area on a 1 mm x 1 mm copper mesh, the fiber is patterned shown in figure 2.7.

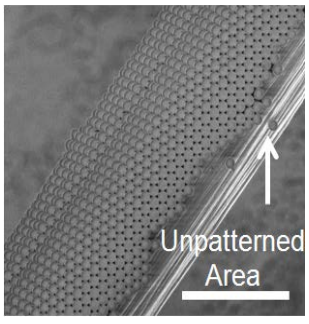

Figure 2.7: SEM image of colloidal array on unsupported region of copper grid. An SEM image of carbon fiber covered with a 500 nm PS colloidal array while the fiber was in the free standing region of the copper grid. Scale bar = 5 μm. Figure reproduced from Pendergraph *et al.* [71]

Although the contact area between the fiber and the substrate prevents complete colloidal coverage around the entire circumference of the fiber, we find that more than 90% coverage (defined as $100*\theta/2\pi$, where θ is the central angle of covered area around the circumference of the fiber) can be achieved. Figure 2.8 is the fiber inverted after coverage on a rigid substrate, where about 9% of the fiber circumference remains uncovered.

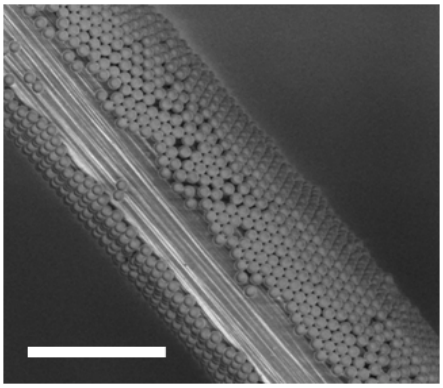

Figure 2.8: SEM image of colloidal array on supported region of copper grid. An SEM image of carbon fiber covered with a 500 nm PS colloidal array while the fiber was directly on the copper grid. Scale bar = 5 μm. Figure reproduced from Pendergraph *et al.* [71]

The copper grid illustrates the ability to coat the fiber without having a continuous substrate, as long as a layer of water remains below the film. However, in order to mitigate potential defects on the fiber from lateral movement of the fiber and inconsistent adhesion of the fiber on the substrate, we chose to place the fibers down on a partially cured Sylgard 184 substrate. In order to have strong adhesion to the surface, it was desirable to have a very compliant material that can make intimate contact. However, the substrate should not allow the fibers to sink too fast where they are completely covered by the silicone matrix. To this end, PDMS was cured at 70^{o}C for 20 minutes, which created a soft solid. The characterization time of the partially cured Sylgard was found

by applying a Maxwell model analysis to this material. The time dependent stress can be modeled with a Maxwell model as the following[72]:

$$\sigma(t) = \sigma_o e^{-\frac{t}{\tau}} \tag{2.1}$$

Where $\sigma(t)$ is the time-dependent stress, σ_o is the initial stress, t is the time, τ is the characteristic relaxation time of the material. For our material, the relaxation time can be observed in this case as the linear portion of the natural logarithmic plot of stress versus time:

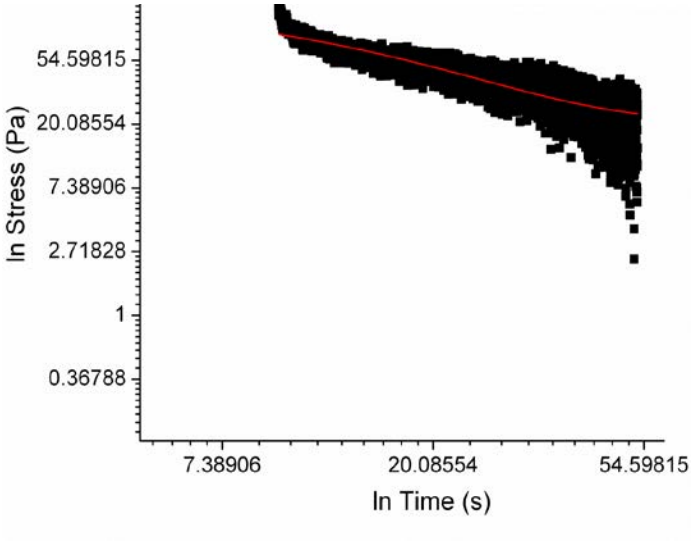

Figure 2.9: Stress relaxation curve of partially cured Sylgard 184. The elastomer was with a 10:1 prepolymer-crosslinker ratio.

This corresponded to a relaxation time (τ) of 13 seconds. The strain for a cylindrical punch in an axisymetric compression can be approximated as the following [75, 76]:

$$\varepsilon \approx \frac{\delta}{a} \tag{2.2}$$

Where, ε is the strain, δ is the displacement into the sample, a is the contact radius of the probe. By combining equations (1) and (2), and applying Hooke's Law (σ=εE) for an elastic material, we find the time-dependent modulus[72]:

$$E(t) = E_o e^{-\frac{t}{\tau}} \tag{2.3}$$

In order to determine the initial elastic modulus of the substrate, we first measured a compliance (or the inverse of the stiffness) of the partially cured Sylgard 184.

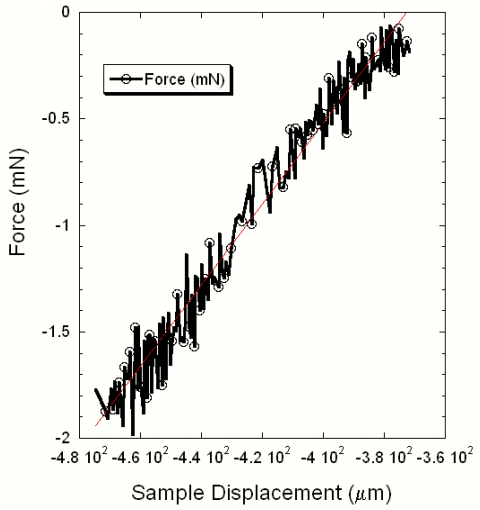

Figure 2.10: A force-displacement curve for the partially cured Sylgard 184. The curve was in the loading portion, before the stress was allowed to relax.

We then applied the following relationship for bulk compliance (C_o) and *a* in equation 2.4.[76]

$$E = \frac{3}{8C_o a} \tag{2.4}$$

However, a bulk compliance can only be assumed if the ratio of the contact radius to sample thickness (h), is much less than one (a/h <<1). In our test, a/h =0.28 and assuming a Poisson's ratio of 0.5, a correction factor for the measured compliance (C) was applied.

$$\frac{C}{C_o} = \left\{1 + 1.33\left(\frac{a}{h}\right) + 1.33\left(\frac{a}{h}\right)^3\right\}^{-1} \tag{2.5}$$

Applying the corrected compliance to equation 2.4, we arrive at an elastic modulus value of 2.0 kPa. By using partially cured Sylgard 184 at this state, the matrix impedes, but

does not prevent the fibers from sinking into the PDMS. After the fibers were placed on the partially cured x-PDMS, the substrate was cured at 70^{o}C for 2 hours to solidify the PDMS. For initial cure times less than 20 minutes, the fibers would sink below the PDMS surface within the processing time (~30 sec.), thus the inverse patterning on the fiber could not be achieved due to a silicone layer blocking the carbon fiber from electrochemical reactions. Similarly, when the initial curing time exceeded 25 min, the surface became too rigid to embed the fibers. This does not preclude the use of the substrate in collecting a colloidal array; however the adhesion of the fibers to the substrate was reduced. The curing time of 20 minutes gave reproducible results for a partially embedded carbon fiber in x-PDMS. Figure 2.11 shows an example of a carbon fiber that was only patterned around its circumference using these procedures with an initial PDMS cure time of 20 min.

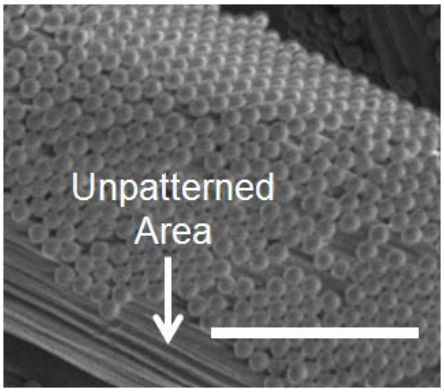

Figure 2.11: SEM image of a 500 nm colloidal array patterned carbon fiber while embedded in Sylgard 184. Scale bar = 5 μm. Figure reproduced from Pendergraph *et al.* [71]

2.4.2 Effect of Colloid Size on Pattern Transfer

The procedure to transfer colloids around a fiber has geometric limitations that are related to the size of the colloid and the fiber. For conformal coverage of the fiber, the number of colloids of some diameter ($D_{colloid}$) should equal the circumference of the fiber:

$$nD_{Colloid} = \pi D_{fiber} \tag{2.6}$$

Where D_{fiber} is the diameter of the fiber and n is the number of colloids. If the ratio between the fiber and colloid diameter is taken, the relationship of the number of colloids of a given diameter that can fit around a fiber is:

$$\frac{n}{\pi} = \frac{D_{fiber}}{D_{Colloid}} \tag{2.7}$$

In the limiting case to enclose a fiber, n = 3, the limiting diameter ratio is 0.95. Roughness on the carbon fiber is apparent from figure 2.12.

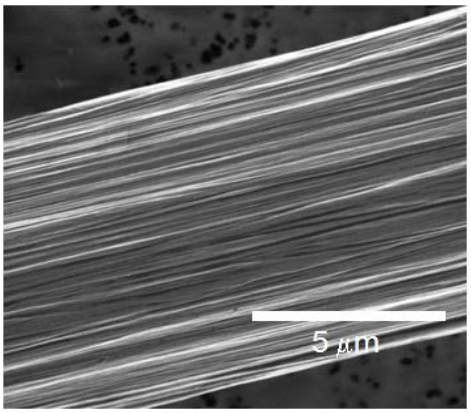

Figure 2.12: SEM image of a bare carbon fiber. Figure reproduced from Pendergraph *et al.* [71]

According to optical profilometry, the fibers used in the experiments had a root mean square (RMS) roughness of 150 nm, measuring down the length of the fiber (61 mm) and 645 nm +/- 230 nm laterally, shown in figure 2.13.

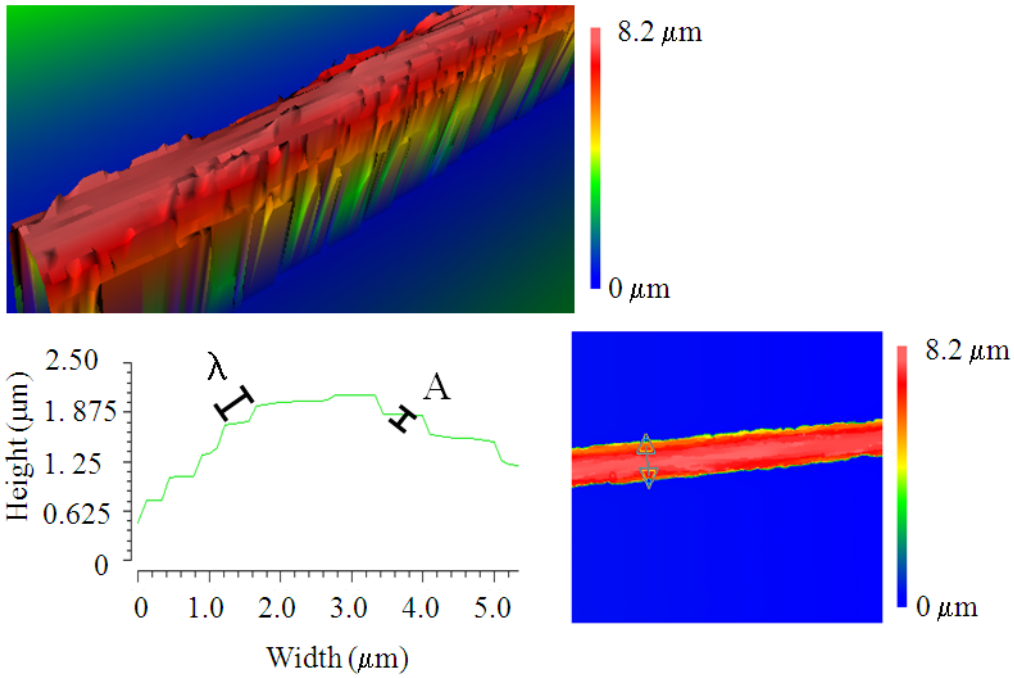

Figure 2.13: Optical profilometry image of a bare carbon fiber cross section. Scale bar = 5 μm. Figure reproduced from Pendergraph *et al.* [71]

The periodicity (λ) and the amplitude (A) of the roughness can be measured directly and then used to calculate a radius of curvature for the roughness on the fiber. The periodicity seen in figure 2.13 gives some indication of what sized particles could potentially fit in the defect, however the periodicity can be related to the depth (amplitude) to give a radius of curvature of the defect. This relationship has been described previously:

$$R \sim \frac{\lambda^2}{2\pi^2 A} \tag{2.8}$$

Where *R* is the radius of curvature of the roughness.[77] The average radius of curvature for these carbon fibers is 140 +/- 103 nm, which is above that of the 200 nm colloids and below the 500 nm colloids. In figure 2.14, there does not appear to be disruption in the ordering of the 500 nm colloidal array due to the roughness on the fiber.

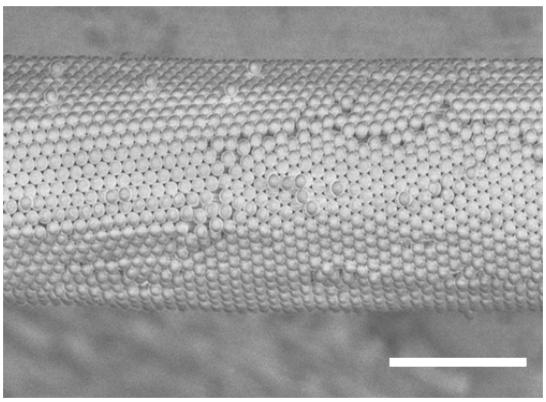

Figure 2.14: SEM image of a carbon fiber covered with 500 nm PS colloidal array. Scale bar = 5 μm. Figure reproduced from Pendergraph *et al.* [71]

However, when the colloidal diameter is reduced to 200 nm, the particles appear to conform to the roughness (figure 2.15).

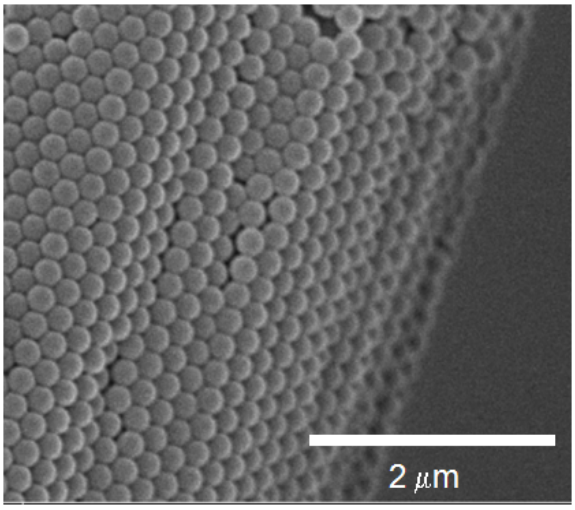

Figure 2.15: SEM image of a carbon fiber covered with 200 nm PS colloidal array. Figure reproduced from Pendergraph *et al.* [71]

In figure 2.15, a 200 nm PS colloidal array was coated over the substrate in a similar manner to the 500 nm array. Unlike the 500 nm particles, which rested on top of the roughness, the 200 nm particles are able to fall into the protrusions of the carbon fiber and conform to the roughness. These differences in the placement of the colloidal array on the fiber roughness are important for subsequent patterning processing that can be used, such as the electrochemical example discussed below. In order to create a consistent pattern around the circumference of the fiber, we implemented electrochemistry where all the pores have equal exposure to the material and the applied potential through the carbon fiber dictates deposition on the surface.

The templated fiber was placed in an EDOT/PSS solution to initiate electrochemical polymerization off the surface of the carbon fiber, which has been established as the working electrode in previous work.[78, 79] After electrochemical polymerization, the fiber was washed with water to remove excess EDOT/PSS and the PS template was then dissolved away with toluene. An electrochemical polymerization time of 900 seconds was ideal for transferring robust patterns. In figure 2.16 an inverse structure using an electrochemical polymerization time of 600 s is shown.

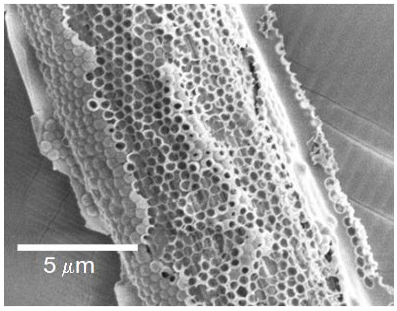

Figure 2.16: SEM image of partially electropolymerized fiber. An SEM image of an inverse PEDOT/PSS structure from a 500 colloidal array with an electrochemical polymerization time of 600 s.

In this case, incomplete patterns were formed across the surface. In figure 2.17, inverse structures from the 500 nm are shown when the electrochemical polymerization time was extended to 900 s.

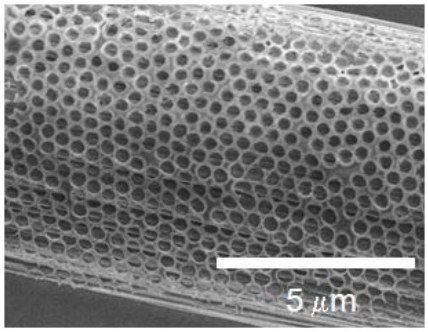

Figure 2.17: SEM Image of Fully Electropolymerized Fiber. A SEM image of an inverse PEDOT/PSS pattern of a 500 nm colloidal array with an electrochemical polymerization time of 900 s. Figure reproduced from Pendergraph *et al.* [71]

Since there was not substantial disruption of the colloidal pattern after 900 seconds, we kept this polymerization time constant throughout the remainder of the study. In figure 2.17, it is apparent the features remain on top of the roughness of the fiber surface, similar to the arrangement of the 500 nm colloids in figure 2.14. Likewise, in Figure 3b the inverse structure is shown on the face of the roughness, similar to the how the 200 nm colloids arrange on the fiber, shown in figure 2.18.

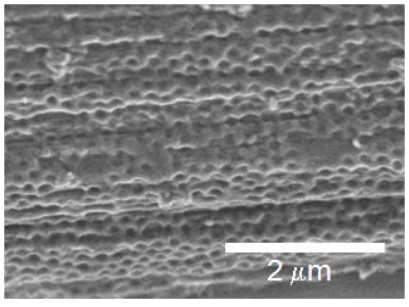

Figure 2.18: SEM Image of Fully Electropolymerized Fiber. An SEM image of the inverse PEDOT/PSS 200 nm colloidal array on the carbon fiber surface. Figure reproduced from Pendergraph *et al.* [71]

The inverse structure from the 200 nm colloids conforms to the roughness similar to the arrangement of the colloids. The correlation between the size scale of the surface roughness and the size of the particles, also affects the corresponding inverse pattern. When a multilayer of colloids is present, the fiber can be electropolymerized and a three dimensional structure can be formed, shown in figure 2.19.

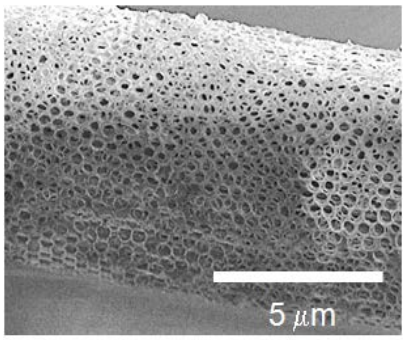

Figure 2.19: SEM Image of Inverse Array Multilayer on Fiber. An SEM image of an inverse 3-D PEDOT/PSS structure on the carbon fiber circumference. Figure reproduced from Pendergraph *et al.* [71]

When partial embedding of the fiber occurs in the x-PDMS substrate, part of the fiber will be patterned and the other part will not be due to substrate obstruction of the EDOT/PSS electrochemical solution. In this case, part of the fiber diameter is patterned and the embedded parts are not, shown in figure 2.20.

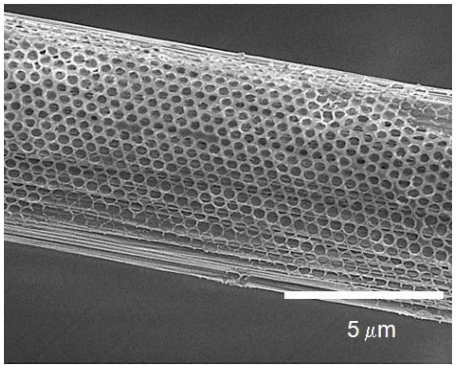

Figure 2.20: SEM Image of Inverse 500 nm Array Partially Patterned Fiber. An SEM image of a partially patterned carbon fiber from a 500 nm colloidal array template. Figure reproduced from Pendergraph *et al.* [71]

Due to the insulating properties of the PDMS within which the fiber is partially embedded, only the exposed regions of the fiber are able to undergo subsequent electrochemistry and deposit other materials on the face. By taking several patterned sections of Figure 2.20, we were able to calculate dimensions of the patterned features from image analysis, shown in figure 2.21.[73]

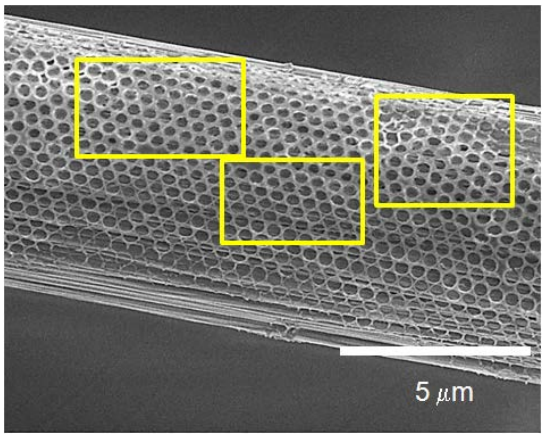

Figure 2.21: SEM Image of Electropolymerized 500 nm Partially Patterned Fiber. Sections taken to evaluate the polymer coverage of the fiber and the dimensions of the pore and wall thickness of the inverse PEDOT/PSS pattern. Figure reproduced from Pendergraph *et al.* [71]

The polymer coverage of the fiber surface was 55 +/- 0.7% in these regions with an average pore diameter of 271 +/- 30 nm and an average wall thickness of 96 +/- 26 nm, for the given reagent concentrations and a electrochemical polymerization time of 900s.

2.5 Conclusions

In conclusion, we have developed a new method of patterning carbon fibers through colloidal lithography. Colloidal arrays were draped over immobilized carbon fibers on several different substrates, including both hydrophilic and hydrophobic materials, by taking advantage of a simple fluid-surface velocity-controlled transition. Depending on the mechanical properties of the substrate used, the coverage and exposure of the fiber circumference can be controlled. The conductive properties of the fibers

were advantageous for demonstrating subsequent patterning methods using electrochemistry templated by interstitial sites of the colloidal array. The colloidal template was easily removed under mild rinsing conditions, leaving nanoscale polymer coatings to define periodic patterns of unmodified conductive fiber surface. Although only carbon fibers were tested, we anticipate the colloidal draping method could be applied to a wide range of non-planar geometries. This procedure provides a new strategy to achieve a number of asymmetric patterns on non-planar surfaces. We anticipate these patterning processes to be advantageous for a range of applications from sensing[80] and actuation[26] to drug delivery.[81]

CHAPTER 3

MECHANICAL PROPERTIES AND PATTERNING OF FABRIC COMPOSITES

3.1 Introduction

Patterning materials on flexible substrates remains challenging due to the materials are typically used as well as the geometric constraints of the substrates. Some materials are easily patterned (e.g. Sylgard 184), however they lack mechanical strength that may be desired. Materials such as poly(ethylene terphthalate) (PET) possess this strong mechanical integrity, however require treatment steps or high temperatures and high pressures to form patterns on the surface. Other problems can occur as well such as delamination and dewetting of patterned films on the surface.

In this chapter, we will address several questions pertaining to the mechanical properties and patterning of elastomer fabric composites. First, what are the basic mechanical properties of such composites? Second, how is the structure of the fibers effect the material properties? What are the conditions to form patterns on the resin surface? Finally, what is the stability of the patterns formed on the substrate? Through these questions, a novel procedure was developed to fabricate patterned composites with unique qualities that have not been observed in previous studies.

3.2 Background

Flexible materials are currently in strong demand for a number of applications, such as flexible electronics and biomedical devices, which require conformability to surfaces and stability under large deformations. [63, 68, 82-84] In order to satisfy this challenge, many flexible substrates tend to be very thin to reduce the strain induced by

bending. [29, 85, 86] Poly (ethylene terephthalate) (PET)[27, 62, 85, 87, 88] and poly(ethylene napthalate) (PEN)[87, 89] have been studied extensively due to their toughness and transparency. Although PET and PEN have attractive qualities, there are difficulties with coating these materials, such as delamination and dewetting.[87] Another approach used to achieve large bending deformations for a flexible substrate is to use low modulus materials. Silicone rubber compositions based upon cross-linked poly(dimethylsiloxane), such as Sylgard 184, (referred to as x-PDMS in this paper) have been demonstrated in flexible substrate applications because of its ability to undergo large and reversible strains and its high bending flexibility.[10, 17, 90, 91] Rogers and co-workers have elegantly demonstrated that under appropriate geometric parameters and processing techniques, x-PDMS can be a versatile platform for flexible electronics.[13, 92-97] Despite the attractive features of x-PDMS compositions, they have a much lower elastic modulus than that of PET or PEN, which may be limiting in certain applications where high mechanical loads are necessary.[10, 17]

To take advantage of both a load-bearing material, such as PET or PEN and the low modulus of silicone rubbers, researchers have integrated stiff materials with soft elastomeric gels. Materials such as paper [19, 98-102] or leather and latex [28] embedded in x-PDMS, as well as gels consisting of ionic liquid and single wall carbon nanotubes[103] have been used as flexible supports. Moreover, non-woven and woven fiber fabrics have also been investigated as flexible substrates. Bae and co-workers have demonstrated the use of a robust woven glass fiber-composite system as a flexible and transparent substrate for transistors and solar cells.[104] However, all the aforementioned findings focus on the device fabrication and lack measurement on the mechanical properties of the substrate.

Furthermore, these reports discuss a two-step patterning approach that involves evaporation or printing of materials onto the substrate rather than directly patterning the substrate material.

In this work, we evaluate the mechanical properties of fabric composites which can serve as an alternative for flexible, patterned substrates. In contrast to much of the previous work where substrates were designed to be either flexible or flexible and stretchable, we investigate substrates with remarkable flexibility as well as high in-plane stiffness, a unique combination of properties that has not been largely investigated. Further, we demonstrate a one-step imprint lithographic procedure to form patterned composites which easily bend but possess high tensile stiffness. Patterned fabric composites are shown to withstand rapid cyclic loading without noticeable degradation of the features. By changing the combination of fabric and resin systems, we demonstrate tunable mechanical properties including high load bearing capacity while maintaining a lower bending modulus. Through this evaluation, these unique properties are discussed in order to provide new, flexible substrate for various applications.

3.3 Experimental

3.3.1 Materials

Norland Optical Adhesive 63 (NOA 63) was purchased from Norland Optical. Sylgard 184 PDMS (x-PDMS) prepolymer and crosslinker were purchased from Dow Corning. Nylon fabric was purchased from Jo-Ann Fabric and Crafts. Plain weave 1-k carbon fiber, uni-directional 12k carbon fiber, glass fiber (E-glass) and Kevlar-Carbon fiber fabrics were purchased from Composite Envisions. F-15 Polyurethane resin was purchased from B.J.B Enterprises. Whatman filter paper (high cellulose paper) was

purchased from Fisher Scientific. Polycarbonate grating masters were created from literature[105]. Poly(ethylene-co-tetrafluoroethylene) (ETFE) was generously provided by Saint-Gobain.

3.3.2 Fabrication of Molds

Rectangular line patterns formed on the x-PDMS and polyurethane resins were created by using a mold fabricated according to literature procedure.[105, 106] Briefly, a commercially available digital video disk (DVD-R) was separated in half and the patterned edge was immediately washed with copious amounts of isopropanol to remove the organic ink. After drying, AFM was performed to confirm the removal of the organic ink and the size dimensions of the lines. For Norland Optical patterning, a daughter x-PDMS mold was first created by pouring degassed Sylgard 184 prepolymer and crosslinker (10:1 prepolymer-crosslinker) over the polycarbonate master and then was allowed to sit for 15 minutes at room temperature to ensure the diffusion of prepolymer and crosslinker into the patterns. The total thickness of the x-PDMS replicas was approximately 1 cm. Next, the uncured Sylgard 184 was placed in an oven for approximately 12 hours at 70^{o}C to ensure the Sylgard 184 was cured. Test pattern features were fabricated from an ETFE daughter mold that was formed from thermally imprinting from a silicon master mold. x-PDMS granddaughter molds of the test patterns were formed in the same manner as the polycarbonate molds.

3.3.3 Imprint Lithographic Patterning on Fabrics

Using tape, the fabrics were attached to a sheet of PET to ensure the fabric remains flat to minimize thickness variations. Next, a resin was poured over the fabric, and allowed to sit for one minute to allow the resin to evenly spread over the surface.

The polycarbonate mold was directly applied to the surface of the uncured resin. Another sheet of PET was placed on top of the mold and then a slight pressure of 370 Pa (0.054 PSI) was applied to ensure even spreading throughout the composite. In the case of polyurethanes, an x-PDMS daughter mold of the polycarbonate master or an ETFE daughter mold (depending on the pattern) was used and the composite was allowed to sit for 24 hours before removing the mold. The x-PDMS composites used the polycarbonate master or ETFE daughter mold directly (depending on the pattern) and cured for 72 hours at room temperature, and then cured in an oven for 15 minutes at 70^{o}C. Room temperature cures were preferable because of the thermal expansion coefficient mismatch between the resins and carbon fiber. For NOA 63 composites, NOA 63 was poured into an x-PDMS daughter polycarbonate mold or granddaughter test pattern mold and exposed under UV (λ= 365 nm) for 15 minutes, until the pattern was completely solidified. Next, the same mold was removed from the cured NOA 63 film. Then uncured NOA 63 was poured on a fabric, spread and then the x-PDMS mold that was just used was placed on top of the uncured resin and exposed to UV light. After 15 minutes, the samples were turned over and cured for an additional 15 minutes to ensure that the backside of the sample was completely cured.

3.3.4 Mechanical Testing of Fabric Composites

Mechanical testing was performed on an Instron 5500R. Bending modulus was measured in a three-point bend configuration (span length=1.92 cm) where the sample was 4 cm in length, 1.2 cm wide, and had various thicknesses (ranging from 0.1 mm -2 mm) depending on the fabric used.[106] The sample was cycled five times at a rate of 1 mm/min to a displacement of 1 mm. Tensile modulus was measured under uni-axial

extension. The substrates and composites were cut into a dog bone geometry with a length of 2.6 cm and a width of 0.46 cm and extended at a rate of 1 mm/min until failure.

3.3.5 Cyclic Testing of Fabrics

Rectangular samples (1.2 cm wide x 6 cm long) were cut and taped in between polycarbonate clamps.[106] One side of the fabric composite was clamped to a fixed support and the other end was clamped to a Black & Decker JS660 Orbital Jig Saw. Samples of x-PDMS, PET and plain weave carbon fiber- x-PDMS composite were evaluated in the cyclic testing. Each sample was subjected to 5000 bending cycles in which the patterned features were under compression, then flipped upside down and an additional 5000 cycles were performed with the features under extension; both loadings were performed at an approximate frequency of 10 Hz, controlled by adjusting the voltage applied to the apparatus

3.3.6 Characterization

SEM images (FEI Magellan FESEM) were taken to investigate the surface features and cross section area of the patterned carbon fiber composites. Tensile and bending mechanical testing was performed on an Instron 5500 R.

3.4 Results and Discussion

3.4.1 Mechanical Testing of Patterned Fabric Composites

We compared the fabric composite mechanical properties to other commonly used materials, such as cellulose paper, x-PDMS and PET, by subjecting them to tensile and bending strains. The tensile modulus (E_T) of the samples was determined from a uniaxial extension test and measuring the slope of the stress-strain data. The non-composite x-PDMS (average thickness = 1.75 mm) and PET (average thickness = 0.12 mm) substrates

were tested and their tensile properties were commensurate with previously reported values with a tensile modulus of 1.2 MPa and 3.7 GPa, respectively.[17, 55, 85, 86, 89] Incorporation of x-PDMS into cellulose-paper caused a reduction in the tensile modulus of the sample from 1.1 GPa in cellulose-paper (average thickness = 0.18 mm) to 0.8 GPa in the cellulose-x-PDMS composite (43% vol. paper, average thickness = 0.24 mm). For composite with non-ordered microstructures (e.g. cellulose-paper/x-PDMS) The modulus of the composite (E_c) generally followed the rule of mixtures, where f the volume fraction of the fibers[107]:

$$E_C = E_F f + E_R(1 - f) \quad (3.1)$$

Where E_F and E_R are the modulus of the fiber and resin, respectively. Accordingly, by embedding cellulose paper in a lower modulus material like x-PDMS, the modulus of the composite is reduced.

For composites with ordered microstructures, such as those created with woven fabrics, anisotropic mechanical properties are expected. A uni-directional carbon fiber-x-PDMS substrate (thickness = 0.45 mm, 22% vol. carbon fiber) was tested in two directions to examine the in-plane anisotropy. In the first case, the fibers were oriented orthogonal (transverse) to the pulling and in the second case, the fibers were oriented parallel (axial) to the pulling direction, depicted in figure 3.1.

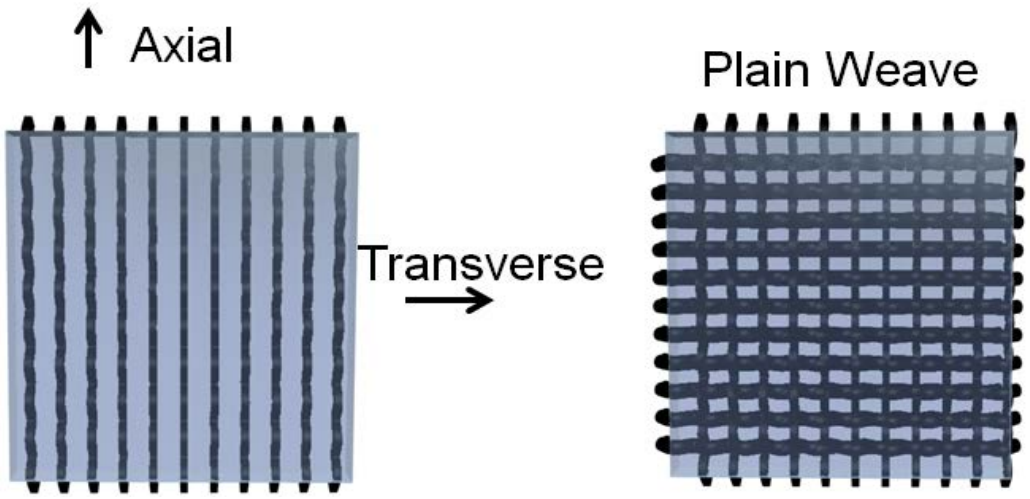

Figure 3.1: **Schematic of Arrangement of Fibers in Fabric Composites. Graphic depiction of the uni-directional carbon fiber composite (left) and the plain weave carbon fiber composite (right). Figure reproduced from Pendergraph *et al.*[106]**

Straining the composite in the transverse direction distributes the stress between the matrix and the fibers, causing the deformation to primarily occur in the soft x-PDMS matrix.[107] This allows the composite to deform easily, similar to x-PDMS, with a tensile modulus of 32.9 MPa. When the sample was strained axially, the tensile modulus was 6.5 GPa. The significantly higher modulus is due to the fact that the fiber and resin go into a state of equal strain. Since there is a large modulus mismatch ($E_F >> E_R$), the majority of the stress is supported by the fiber. An even higher tensile modulus is obtained in the plain weave carbon fiber composite (thickness = 0.24 mm, 34 % vol. carbon fiber) with a modulus of 10.5 GPa. Here, the weave pattern helps to reinforce the fabric against tensile strain.[108] By measuring the tensile modulus, we gained an understanding of the energy density that is required to stretch these composites. In order to guide material design, we wanted to contrast this energy storage to the energy required to deform the same volume in a bending geometry.

The composite bending moduli (E_B) of the materials were determined using a linear elastic relationship for a simply supported rectangular beam with the load concentrated in the center as:

$$E_B = \frac{kL^3}{4bt^3} \tag{3.2}$$

Where L is the length of the span, b is the width of the sample, t is the thickness of the sample and k is the experimentally determined bending stiffness of the sample. PET had the highest bending modulus (6.8 GPa) while x-PDMS had the lowest bending modulus (1.3 MPa), which is similar to the bulk modulus of x-PDMS. Cellulose paper-x-PDMS composite modulus (0.6 GPa) was lower than pure cellulose (1.2 GPa), again due to the incorporation of a lower modulus matrix. Similar to the tensile testing, the modulus of the carbon fiber composites was dependent on the direction of the fibers with respect to the orientation of the span length. When the composite was bent in the transverse direction with respect to the fibers, the matrix properties dominated the bending behavior, and the modulus approached that of x-PDMS (7 MPa). However, when the fibers were aligned axially to the span length, the bending stiffness was raised substantially and the uni-directional carbon fiber exhibited a much higher modulus at 1.5 GPa. The plain weave carbon fiber fabric had a relatively high bending modulus (0.7 GPa), however this value is over an order of magnitude lower than its tensile modulus (10.5 GPa). The compilation of the tensile and bending moduli is shown in figure 3.2.

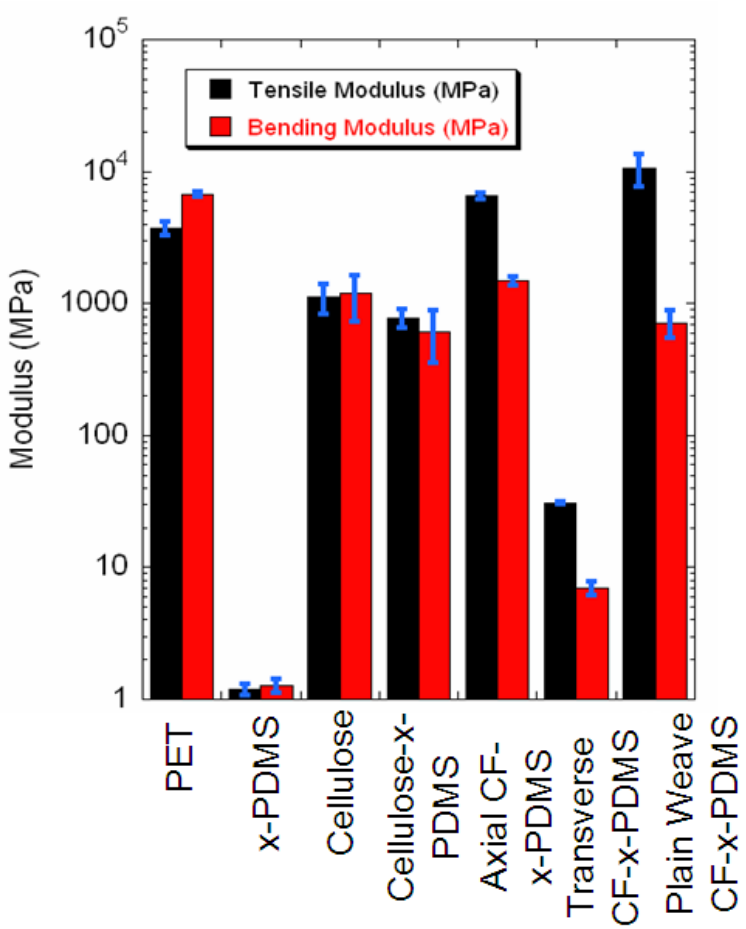

Figure 3.2: Tensile and Bending Modulus Compendium. Figure reproduced from Pendergraph *et al.*[106]

By understanding the differences in the moduli for tension and flexure, we can implement these properties in order to design materials for appropriate flexibility. In Figure 3.3, the ratio of the tensile modulus to the bending modulus is shown for the composites and materials tested.

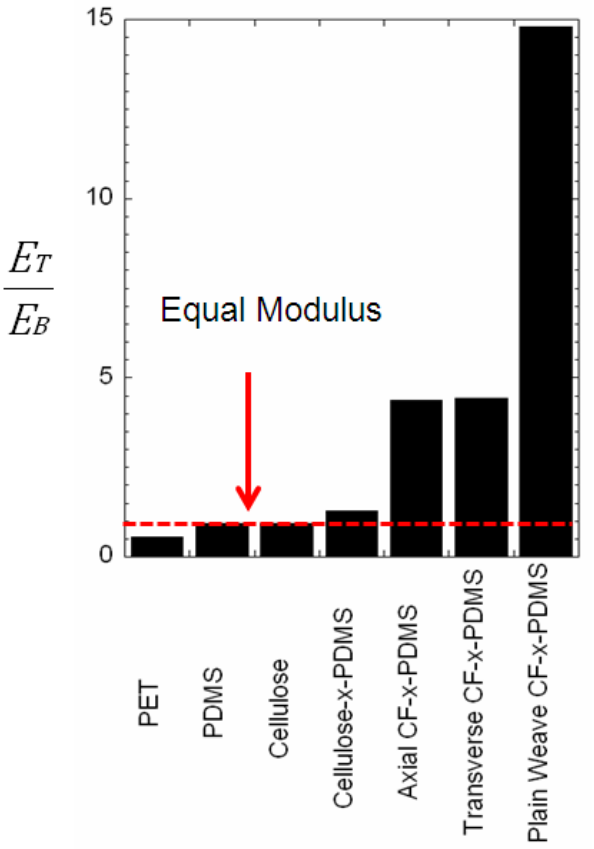

Figure 3.3: Modulus ratio plot. Tensile to bending modulus ratio of all of the samples tested, the dotted line denotes the value of equal tensile and bending modulus. Figure reproduced from Pendergraph *et al.*[106]

As expected, x-PDMS and PET approach unity as these are homogenous materials with no reinforcement or other material affecting the anisotropy of the film. For these types of materials, the bending flexibility comes at the cost of reducing the modulus of the material or keeping a very thin geometry. Both cellulose paper and cellulose paper-x-PDMS also exhibited a ratio that approached unity, which was also expected because the fibrous network was not an ordered microstructure like the other fabric materials. The plain weave carbon fiber exhibited the largest tensile to bending ratio of 14.8, which is a combination of several factors of the composite. Having a matrix with a much lower modulus is crucial for the fiber composite to retain this high

difference of stretching to bending. The tensile strain is limited by the stiffer component of the composite when the sample is strained axially. However, in bending, the composite bending modulus is not only a property of modulus mismatch and relative volume fraction, but also the position of the components. In particular, the position of components relative to the neutral axis is a factor in determining bending resistance. The neutral axis for our composites is determined by a relationship:

$$E_F \int_{A_F} y dA + E_R \int_{A_R} y dA = 0 \quad (3.3)$$

Where *y* is the distance of the centroid of the material to the neutral axis of the composite, A_F and A_R are the cross-sectional area of the fiber and the resin, respectively. In our composites, the neutral axis is centered on the middle of the fabric. When the composite is in flexure, the fibers are subjected to the least amount of strain and the matrix will have a larger strain. The greater strain is therefore present in the lower modulus x-PDMS, thus requiring little energy to bend to a given radius of curvature. This allows substrates to possess a higher thickness, yet maintain similar flexibility.

The anisotropy and direction of the fabric also allows for stiffness control in the plane of the substrate.[109] Due to the symmetry of the plain weave carbon fiber, the mechanical properties are symmetric within the plane of the fabric. The asymmetric weave pattern (i.e. uni-directional fibers) allows these properties to be different within the plane of the fabric, depending on the alignment of the fibers.[109] For the uni-directional carbon fiber composite, there was a substantial difference between the modulus when the composite was strained axially versus transversely relative to the fiber direction. Therefore, if the substrate needs to accommodate strain in one direction of the plane, it can easily be tailored to do so while strongly resisting in the other direction within the

same plane. This control of the tensile stress distribution of the composite within the plane is not available in homogenous planar substrates.

3.4.2 Lithographic Patterning and Stability of Fabric Composites

The scope of this study was to demonstrate the ability and advantages of fabrics as a substrate and to understand the materials properties of fabric composites in order to create tunable composites for use as flexible substrates. Inspired by previous work by our team, we aimed to further evaluate the mechanism in which these composites can be very resistant to tensile forces but maintain high flexibility.[30] Our method of creating these fabric composites is described in Figure 1a, and allows for surface patterning via imprint lithography. By imprinting directly into the resin and curing, stable patterns are formed without the need to account for surface instabilities (Figure 1b), unlike many polymer substrates where surface modification is required to provide stable coatings.[62] The dimensions of the line pattern mold for our sample was measured by AFM and had a line width of 400 nm with a periodicity (λ) of 750 nm, a height of 150 nm, shown in figure 3.4.

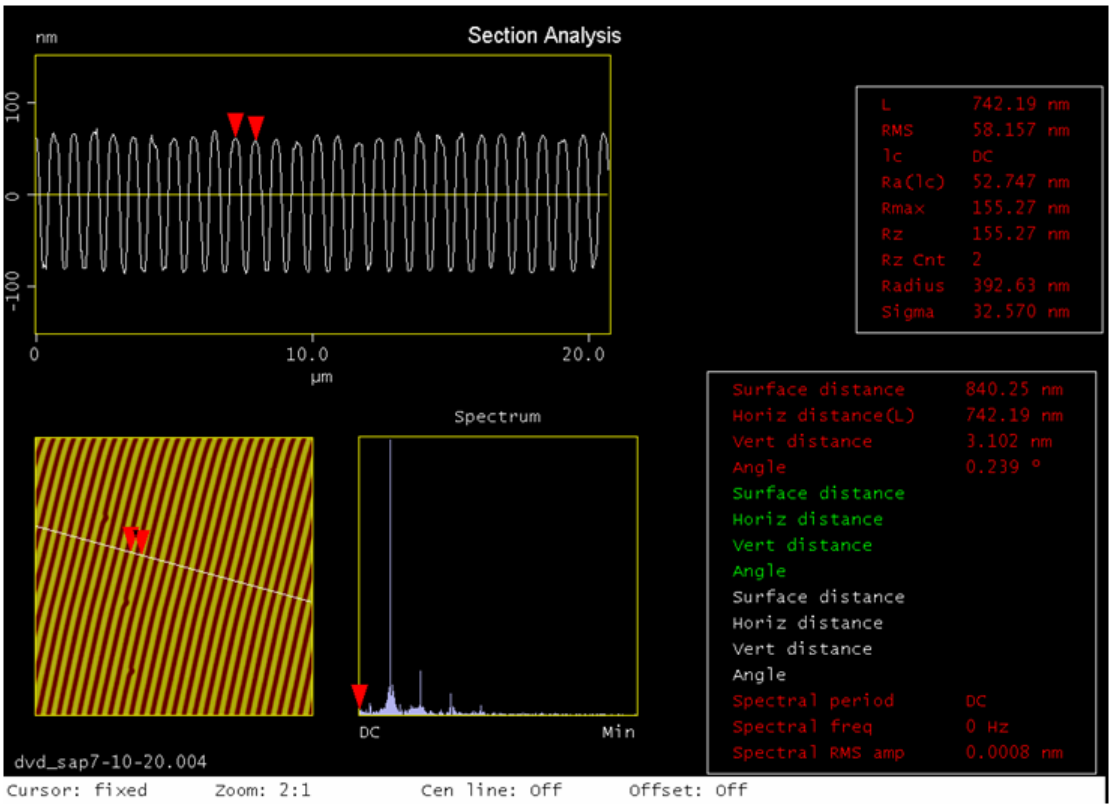

Figure 3.4: AFM image of line pattern mold. AFM cross section area of mold used for imprinting into fabrics. Figure reproduced from Pendergraph *et al.*[106]

After imprinting, we found, λ remained the same at 750 nm; however the line width was reduced to 350 nm, Figure 3.5.

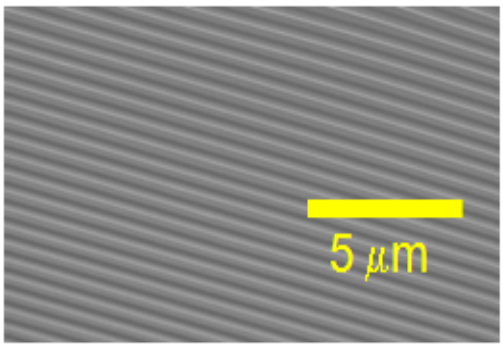

Figure 3.5: SEM image of imprinted carbon fiber composite. Figure reproduced from Pendergraph *et al.*[106]

An SEM image of the fabric composite cross section illustrates the penetration of the resin through the fabric and the resulting line pattern formed on the surface, shown in figure 3.6.

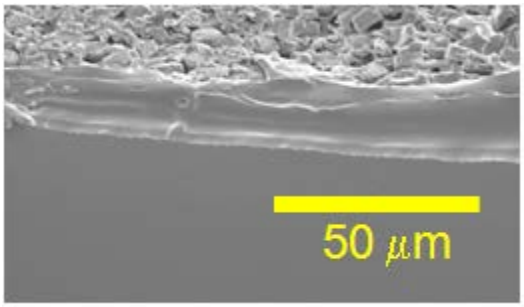

Figure 3.6: SEM image of x-PDMS/Carbon cross-section. SEM image of cross section of carbon fiber/x-PDMS fiber composite. Figure reproduced from Pendergraph *et al.*[106]

If we examine a larger cross section area, shown in figure 3.7, the residual layer of x-PDMS underneath the patterned face was found to be 38 μm +/- 18 μm.

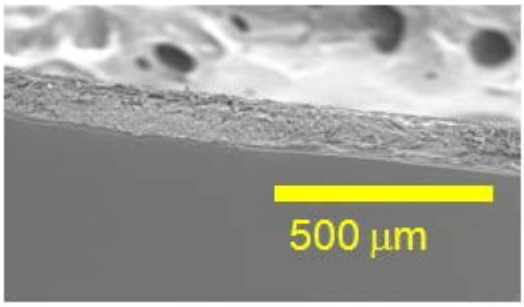

Figure 3.7: SEM image of fabric/resin cross-section far magnification. SEM image of cross-section of carbon fiber/x-PDMS fiber composite, the residual layer was measured between the patterned surface and the fibers. Figure reproduced from Pendergraph *et al.*[106]

Imprint lithography can be used for the rapid replication of features[110] and fabrics can in principle be easily scaled to large volumes in roll-to-roll fabrication processes. Furthermore, this patterning technique can be extended to a number of fabrics and resins, shown in Figure 3.8.

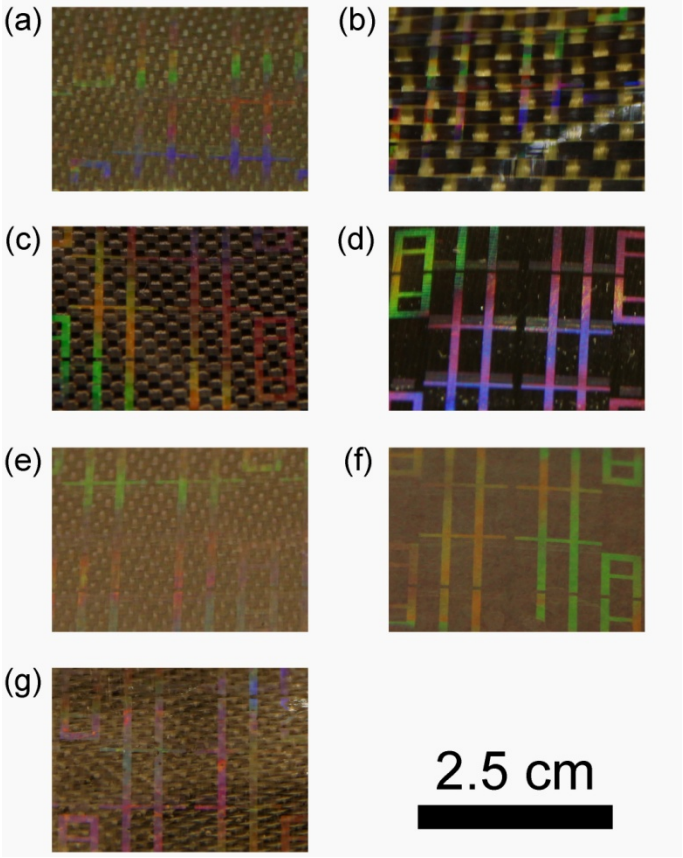

Figure 3.8: Macroscopic photographs of various fabric/resin combinations. (a) E-glass/x-PDMS, (b) Kevlar-Carbon fiber/x-PDMS, (c) Plain weave Carbon Fiber/x-PDMS, (d) Nylon/x-PDMS, (e) E-glass/Polyurethane, (f) Cellulose paper / x-PDMS, (g) E-Glass/Norland Optical 63. Figure reproduced from Pendergraph *et al.*[106]

x-PDMS and polyurethane are two examples of thermally curable materials that can be used with various organic and inorganic fabrics (Figure 3.8 a-f). The formation of a planar substrate is not limited to thermally cured resins; UV curable resins such as Norland Optical can also be utilized (Figure 3.8 g).

To test the stability of the patterned lines under mechanical deformation, we designed a custom-made cyclic testing apparatus to subject a rapid deformation, shown in figure 3.9.

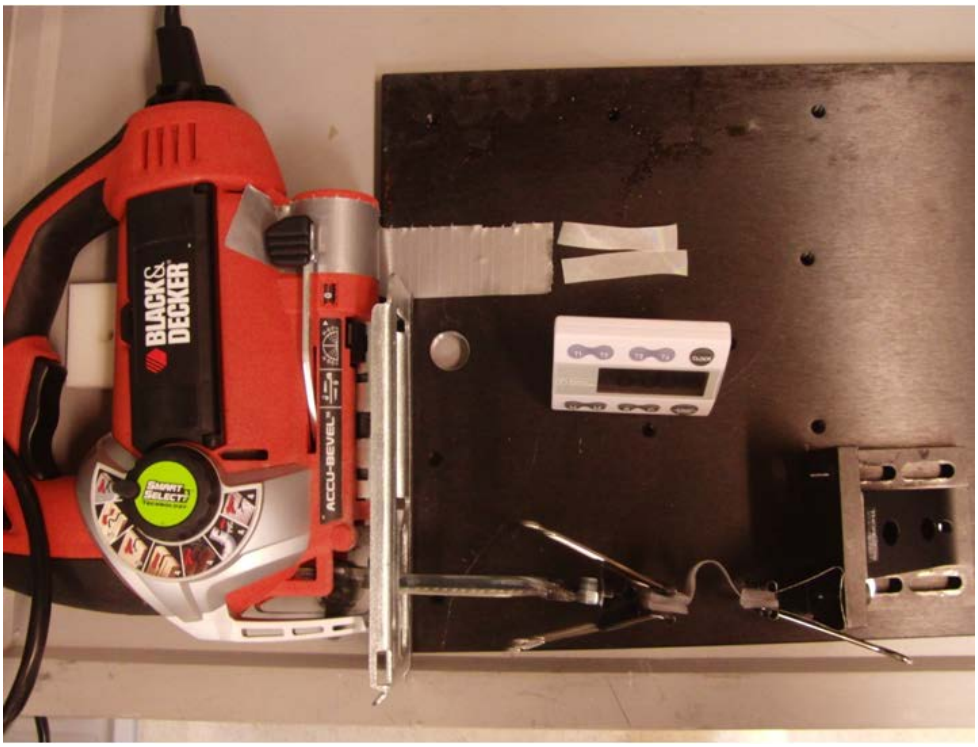

Figure 3.9: Photograph of cyclic testing apparatus. Custom made cyclic testing apparatus with a Black&Decker® jig-saw. The composite was cycled to a bending radius of 3.1 mm through a rapid deformation (10Hz) over 10,000 testing cycles

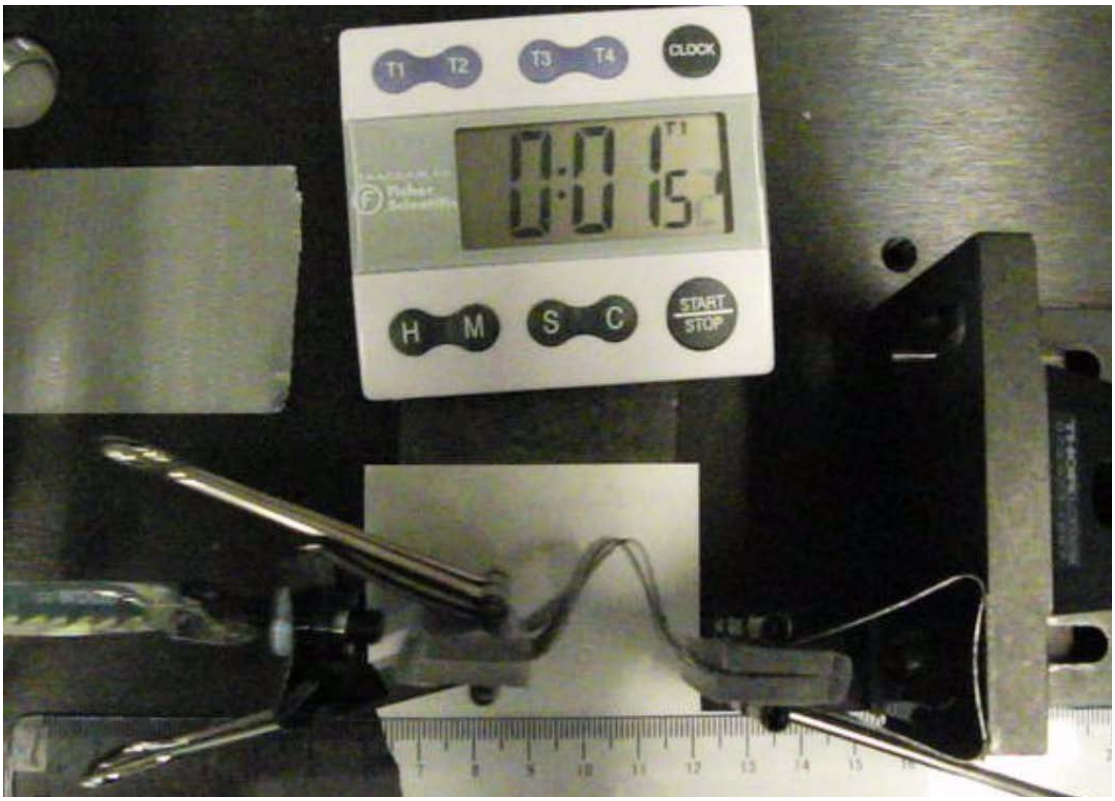

Figure 3.10: Photograph of cyclic testing apparatus. Cyclic testing of multiple samples at a frequency of approximately 10 hz over 10,000 cycles. Figure reproduced from Pendergraph *et al.*[106]

SEM micrographs of the sample before and after the cyclic testing show no apparent change in the size or shape of the patterns after testing, shown in Figure 3.11.

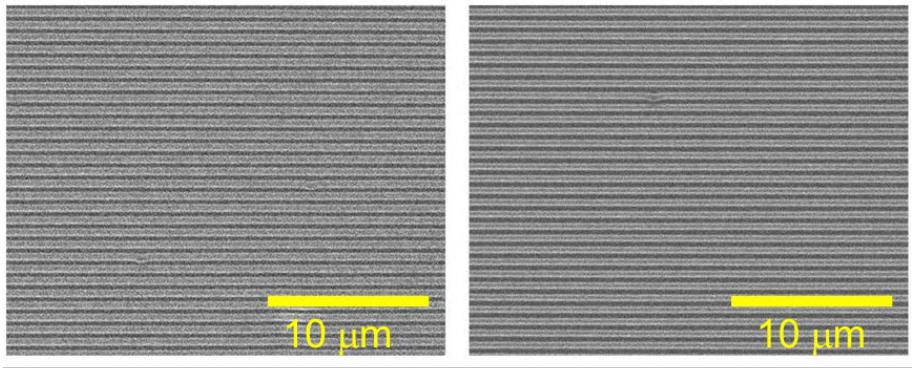

Figure 3.11: SEM image of x-PDMS/carbon fiber composite before/after cyclic mechanical testing. Image before (left) and after (right). Figure reproduced from Pendergraph *et al.*[106]

Although the sample was bent to a small radius (~3 mm), the maximum strain imposed on the patterned features was only 5.7% because of this sample's thickness (360 μm), which is well within the elastic limits of x-PDMS.[17, 94] Testing the mechanical properties of free-standing samples of x-PDMS with comparable thicknesses was not possible due to extensive sagging and self-adhesion in the flexure test. Furthermore, the features on the patterned composite did not change regardless if the applied strain was compressive or extensional.

3.5 Conclusions

We have described a versatile and facile method for producing patterned, flexible composite substrates. By using imprint lithography, patterning is incorporated directly into the composite fabrication step, eliminating the need for planarization required in conventional flat substrates. These 400 nm patterns are mechanically stable after 10,000 rapid deformation cycles in both extension and compression. A number of fabric and resin combinations were tested to demonstrate the versatility of this method. Compared to commonly used flexible substrates, these elastomer-fiber composites have superior tensile moduli while still maintaining comparable or superior bending flexibility. By varying the fiber alignment, in-plane anisotropy was observed in the tensile and bending modulus that can be easily adjusted by changing the fabric geometry (uni-directional vs. plain weave). We anticipate that this will provide superior attributes in load-bearing applications that are not possible with current materials, such as Sylgard 184 (x-PDMS) and PET. Finally, we have demonstrated the superior in-plane strain resistance that can be achieved while maintaining high flexibility. Fabric reinforcement provides the ability to resist tension strongly, yet allow comparable or superior flexibility given a set

geometry. We anticipate these features to provide robust materials for flexible electronics as well as biomedical devices.

CHAPTER 4

ADHESION OF PATTERNED FABRIC COMPOSITES

4.1 Introduction

The design of robust, reversible adhesives has been studied with immense interest in recent years through modification of interfacial chemistry and geometry. One example is bio-inspired adhesives which have mimicked the fibrillar features found on the adhesive toe pads of organisms such as the Tokay Gecko to control adhesion.[5-9, 111] Aside from long, thin compliant structures, other topographies such as wrinkles and interlocking structures have also been implemented to control adhesion strength.[4, 54, 77, 112-117] Studies have been conducted with normal, peel and shear adhesion of bio-inspired surfaces[3, 5-7, 9, 118, 119], as well as patterned soft materials, in general.[120-122] While advantages have been highlighted in all of these soft fibrillar like structures, limitations are also acknowledged in terms of their overall loading capacity. Specifically, patterned structures that are comprised of soft materials can make intimate contact but lack high stiffness to achieve high loads.

Recently, elastomeric fabric composites have been demonstrated to achieve high shear adhesion forces, while remaining reversible.[30, 47] This advantageous balance of properties arises because the soft elastomer can establish intimate contact on the micron and sub-micron length scales while also allowing for the fabric to drape and maintain contact at larger sizes on non-ideal substrates.[106] In addition, the rigid fibers of the fabric minimize deformation, leading to a high adhesive force capacity. Adhesion through these fabric composites relies primarily on material elasticity and reversible non-specific surface interactions such as van der Waals forces, thus reducing material

constraints on the design of the adhesive. However, this general design concept has the potential for further modification of surface topography to add increased functionality.

In recent work by Chaudhury and co-workers, they described how incisions and discontinuities in a film can lead to an increase in peel adhesion.[3] They examined the role of line discontinuities on the effect of crack propagation in peel adhesion of elastomers and demonstrated that crack blunting can lead to substantial adhesion improvements. Specifically, they highlight two factors: first, the orientation of the line incisions should be orthogonal to the peel direction (or parallel to the crack front). Second, the incision spacing should be less than a critical stress decay length. Understanding how the crack propagation occurred in these types of patterns, the researchers devised more complex topographies to enhance the adhesion through a crack blunting mechanism.[3]

In the previous chapter we have demonstrated the ability to pattern elastomeric fabric composites. In this chapter we will examine the effects of the patterns on the fabric composites and how the size and the orientation of the lines affect the adhesion.

Here, we expand the general design concept of elastomeric fabric adhesives through surface patterning to demonstrate further control of shear adhesion force capacity. Specifically, we demonstrate the facile use of topographical line patterns to enhance shear adhesion strength up to almost 40% compared to the non-patterned composite material. By orienting the line patterns orthogonal to the crack propagation, higher adhesion was achieved by slowing catastrophic failure of the interface through crack blunting.

4.2 Experimental

4.2.1 Materials

Polydimethylsiloxane (PDMS) elastomer Sylgard 184™ (referred in this paper as x-PDMS) was purchased from Dow Corning. Plain-weave carbon fiber 1-k fabric was purchased from Composite Envisions. Rewritable compact discs (CD) and digital video disk (DVD) were purchased from Verbatim.

4.2.2 Instrumentation

Mechanical testing was performed on an Instron 4400R and 5500R with a 50 N load cell. Atomic Force Microscopy (AFM) was performed on a Digital Instruments Nanoscope III in tapping mode under ambient conditions. Contact adhesion testing was performed on a custom contact adhesion testing instrument.[123]

4.2.3 Fabrication of Patterned Fabric Composites

CD and DVD patterned fabric composites were fabricated by literature procedures.[106, 124] Briefly, the CD mold was fabricated by removing the foil on top of the CD and then washing immediately with copious amounts of isopropanol. After the organic ink was removed, the sample was dried with a stream of air. For DVD molds, the disc was separated into two pieces and then the patterned section was washed with copious amounts of isopropanol. Both CD and DVD discs have a radius of 6 cm. Sylgard 184 was mixed at a 5:1 prepolymer-crosslinker ratio and degassed to remove air bubbles. After, a mold was then placed on a sheet of Poly(ethylene terphthalate) (PET). Sylgard 184 was then poured into the mold. Next, a piece of plain-weave carbon fiber was placed on top of the Sylgard 184. More Sylgard 184 was poured on top of the fabric, until completely covered and another piece of PET was placed on top of the resin covered

fabric. The composite was allowed to cure for 72 hours at room temperature, followed by a 1 hour cure at 70^{o}C. Finally, the mold was removed leaving a patterned fabric composite. For the case of the non-patterned substrate, Sylgard 184 was poured on top of the carbon fiber fabric and placed between two sheets of PET and cured in the same method as the patterned composites.

4.2.4 Adhesion Testing of Fabric Composites

Fabric composites were tested for adhesion testing by clamping the end opposite of the testing area between two pieces of polycarbonate. The patterned area size was kept to approximately 2 cm^2 for all samples. A distance of 4 cm between the bottom of the patterned feature and the top of clamping area was held constant through all adhesion testing. The polycarbonate grips were then clamped into to the fixed end of the Instron. Next, a piece of glass was cleaned by manual washing with commercial soap and then dried under a stream of air. The cleaned piece of glass was then clamped into the moving head of the Instron set up. The testing area was then attached by hand to the glass slide and then the testing was initiated with varying testing velocities.

4.2.5 Microscopic Adhesion Testing of Fabric Composites

To image the propagation of interfacial failure at sufficiently high resolution, lap shear adhesion tests were performed on a custom-designed instrument that was fixed below an optical microscope. Specifically, fabric composites were tested by clamping a cleaned 75 x 55 mm glass slide to a rigid stand fixed to a breadboard table. The unsupported edge of glass slide was then placed underneath the microscope objective (2.5 x magnification) with a Zeiss AxioTech Vario optical microscope. The bottom of the fabric composite was clamped to another rigid stand, which is also fixed to a breadboard

table and the testing region of the composite was brought into contact on the bottom side of the glass slide. After the sample was in focus, the sample was pulled horizontally at a testing velocity of 5 mm/min.

4.2.6 Modulus Measurement of x-PDMS

Mechanical properties of x-PDMS were evaluated through tensile testing on an Instron 4400. The samples were cut into dog-bone samples and pulled at 5 mm-min.

4.2.7 Determination of G_c for bulk x-PDMS

To provide a baseline measurement of the adhesion between the x-PDMS elastomer and glass, measurements of the mode I critical energy release rate, G_c, were performed using a custom built contact adhesion testing instrument. A glass hemispherical probe (radius = 5 mm) was brought into contact with the x-PDMS substrate at rate of 5 mm/min to a load of 10 mN and then withdrawn at the same rate, while the contact force, relative displacement, and contact area were monitored continuously. An effective G_c was then determined from the critical pull off force using the JKR relationship,

$$G_c = \frac{2P}{3\pi R} \tag{4.1}$$

Where R is the radius of curvature of the glass probe and P is the maximum tensile load at adhesive separation. Although it is known that Gc is velocity dependent for elastomer interfaces in general, for this study we limit our characterization to a single velocity which is appropriate for drawing comparisons to the lap shear experiments.

4.3 Results and Discussion

4.3.1 Shear Adhesion Testing

Shear adhesion experiments were performed on five different samples, a non-patterned plain-weave carbon fiber/x-PDMS sample, as well as two different spacing rectangular patterns, in two different orientations. For the patterned samples we defined the lines as being oriented "parallel" when the lines were oriented along the testing directions and "orthogonal" when the lines were perpendicular to the testing direction. The fabric composites patterned from the DVD features had a periodicity (λ) of approximately 750 nm, a depth (*d*) of 150 nm and a spacing width (*s*) of approximately 350 nm (figure 4.1).

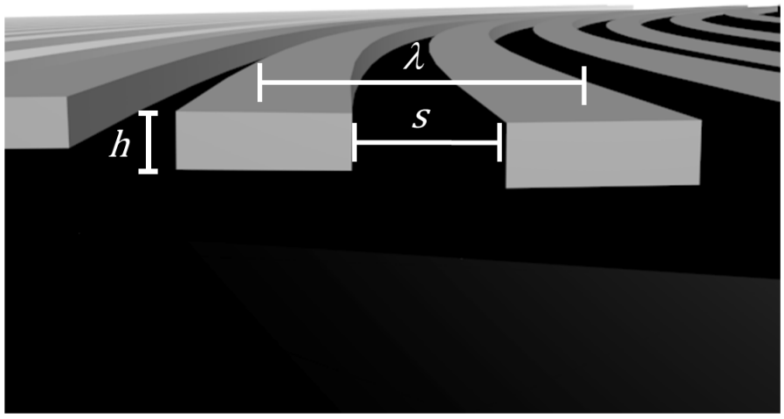

Figure 4.1: Schematic of the dimensions of the pattern on the surface. Figure reproduced from Pendergraph *et al.*[124]

The CD features had a periodicity of approximately 1500 nm, a depth of 200 nm and a spacing width of approximately 600 nm, according to AFM (figure 4.2).

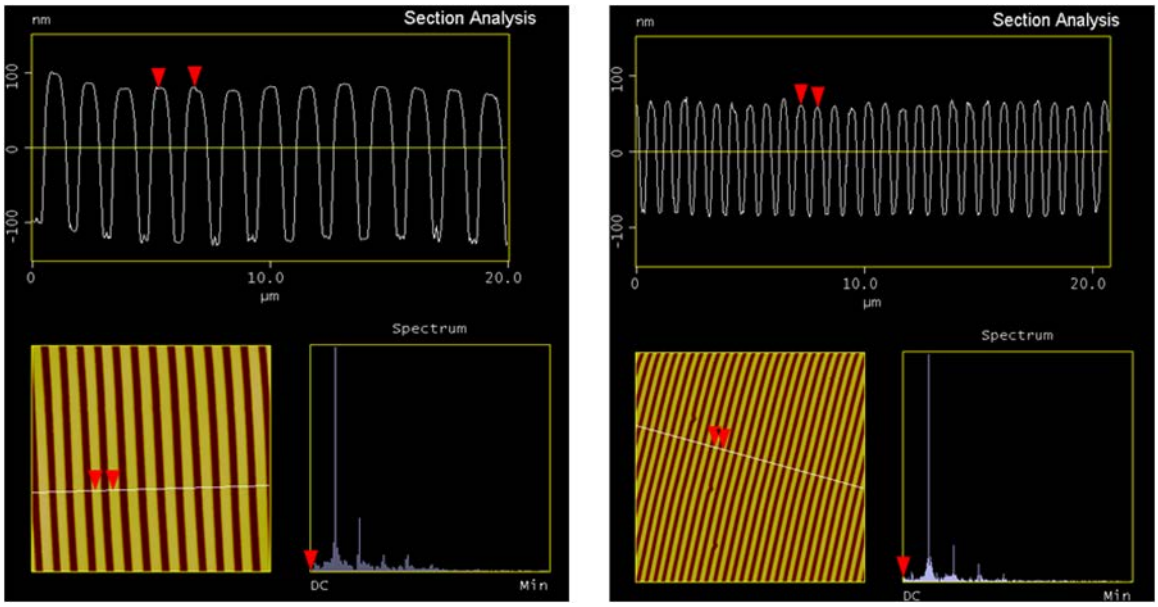

Figure 4.2: AFM images of mold dimensions for patterning. AFM images of the CD mold (left) and DVD mold (right). Figure reproduced from Pendergraph *et al.*[124]

The use of the CD and DVD patterns enabled the rapid and reliable replication of these sub-micrometer dimensions.

Since the patterns originated from a circular pattern we needed to consider how the orientation of the lines changes as a function of sample size and geometry. The sector angle gives the range of angles the line will deviate from the testing direction. The sector angle can be expressed as a function of the diameter of the CD or DVD template (D) and the chord length (a):

$$\theta = 2\sin^{-1}\left(\frac{a}{D}\right) \tag{4.2}$$

The chord length for the orthogonal example is related to the width, and conversely, the length of the sample for the parallel orientation. The angle of an arbitrary line relative to a given position of the sample was determined since both *a* and *D* were known in the sample construction, shown in figure 4.3.

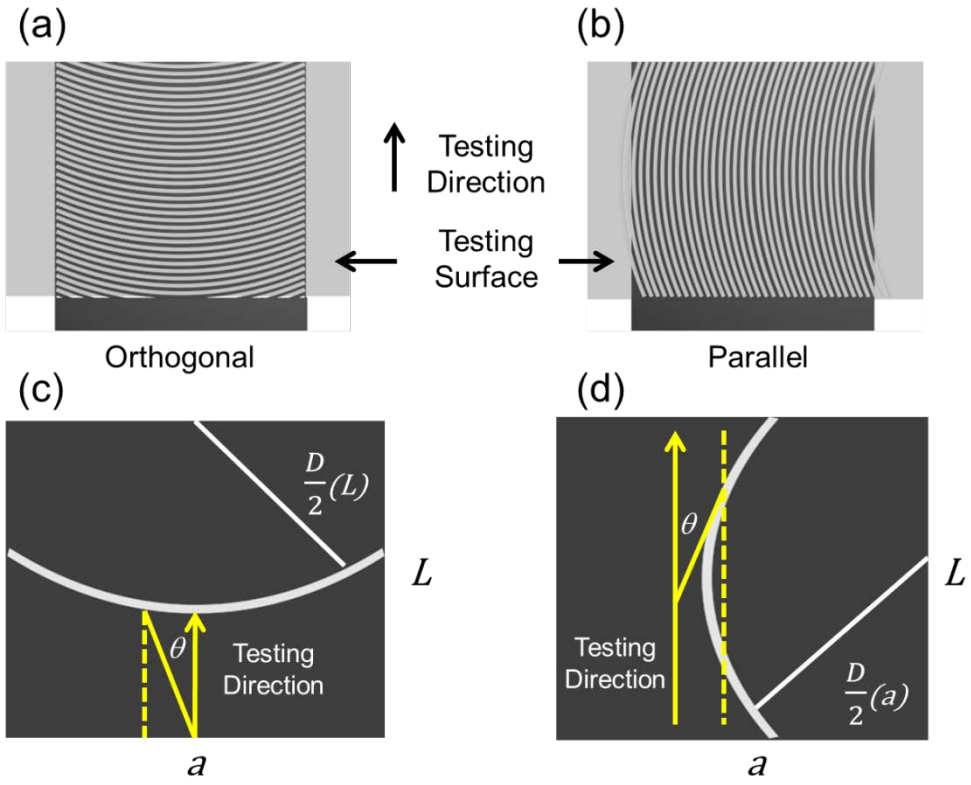

Figure 4.3: Angle dependence of lines relative to radial position. The angle of the applied force to the line relative to position on the substrate. The angle of a given location of the line can be related to the sector angle of the CD or DVD template through equation 2 for the orthogonal orientation (a) and parallel orientation (b). Figure reproduced from Pendergraph *et al.*[124]

The angle of the line relative to an idealized line direction typically varied from 0 degrees to +/- 17.5 degrees (corresponding to a total sector angle of 35 degrees), depending on the radius of curvature of the line and relative position in the chord length. A total sector angle of 90 degrees or higher (from an idealized line direction) would lead to line features on a single pad which have both parallel and orthogonal orientations. This non-negligible mixture of line orientations would occur at (a/D) values between 0.806 and 1; for our samples, the values for (a/D) were limited between 0.075 and 0.10. Therefore, despite the curvature of the lines, at the size scales investigated here the two line

arrangements remained distinct from each other in terms of the angles exhibited during testing.

After the patterns were fabricated, the samples were clamped and the testing area was applied to a glass slide until the disappearance of the diffraction grating (figure 4.4).

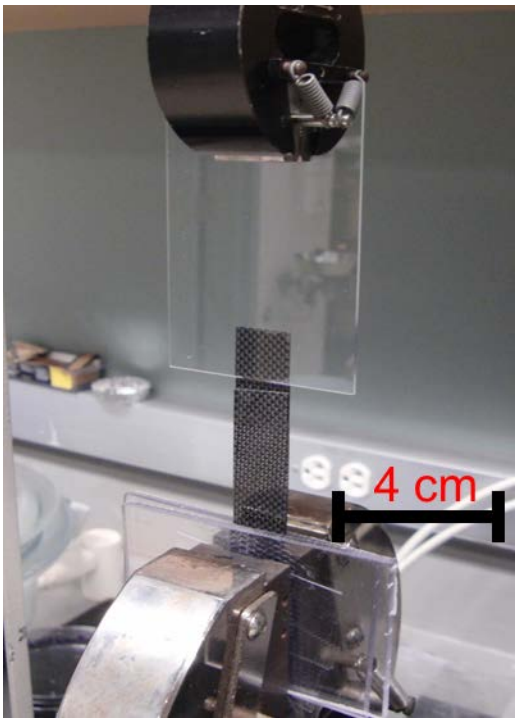

Figure 4.4: Adhesion testing set-up. Picture of a patterned fabric composite and in contact with the testing surface prior to applying load. Figure reproduced from Pendergraph *et al.*[124]

The disappearance of the light diffraction indicated intimate contact, where both the top and bottom of the line features were in contact and remained stable until the sample was strained. The sample was then loaded until a maximum critical force (F_C) was reached and the adhesive subsequently separated from the substrate completely.

4.3.2 Effect of Pattern Orientation on Critical Force

Representative plots of the 5 different patterned surfaces are shown for 5 mm/min testing rate, along with the corresponding adhesive stress capacities (F_C/A, where A is the projected contact area), in figure 4.5.

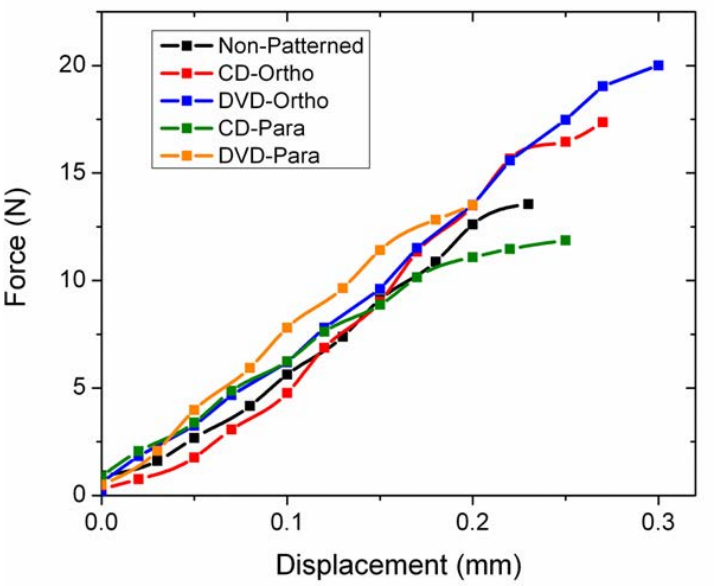

Figure 4.5: Force vs. Displacement plot. Force vs. displacement curve for the five different fabric composite patterns tested at 5 mm/min. Figure reproduced from Pendergraph *et al.*[124]

The orthogonal patterns demonstrated different shear adhesion values compared to the parallel and the non-patterned samples. The CD and DVD samples exhibited a 20% and 37% increase in adhesion, respectively, relative to the non-patterned substrate. In order to discern the source of the enhancement of the orthogonally patterned features, we first implemented a previously reported general force scaling relationship for reversible adhesion[30, 47]:

$$F_c \sim \sqrt{G_c}\sqrt{\frac{A}{C}} \tag{4.3}$$

Where F_c is the critical adhesive force, G_c is the critical strain energy release rate, A is the area of contact and C is the compliance of the sample in the loading direction. From our previous work with elastomeric fabric composites, we have shown that adhesive failure, or interfacial fracture, occurs in a single step (i.e. unstable crack propagation) when F_c is reached. Since the samples had identical resin materials and processing conditions, G_c is unlikely to be the differentiating component to the adhesion discrepancies. The contact area (A) and compliance of the samples (C) was similar and relatively invariant, even with varying velocities (shown in figure 4.6), and therefore is unlikely to be the source of variance in the adhesion performance.

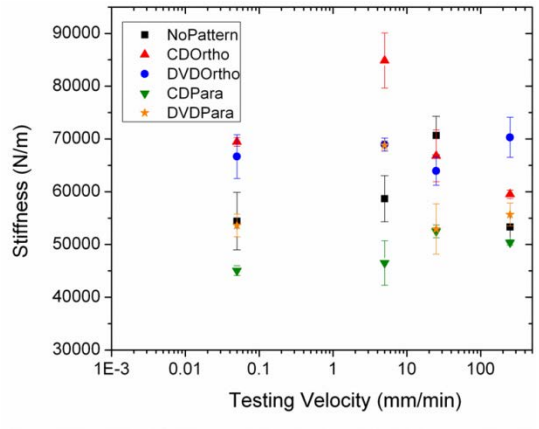

Figure 4.6: Stiffness vs. velocity plot. Stiffness of patterned samples as a function of testing velocity. Figure reproduced from Pendergraph *et al.*[124]

We attribute the change in force capacity to the ability of the orthogonally patterned samples to initially blunt crack growth, shown in (figure 4.7).

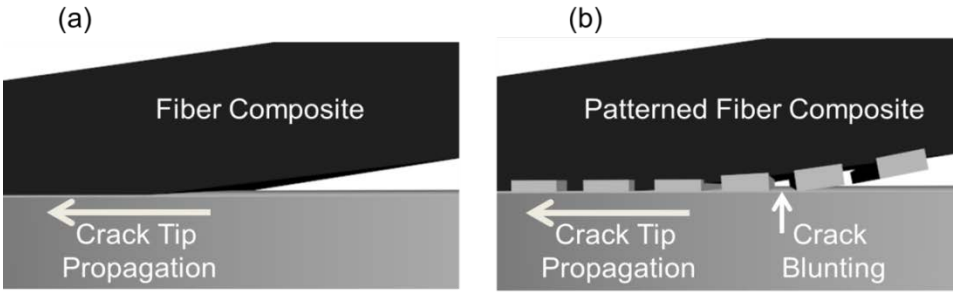

Figure 4.7: Figure of crack propagation at interface. Schematic of the crack propagation in an unpatterned sample (a) and an orthogonally patterned sample (b). Figure reproduced from Pendergraph *et al.*[124]

This blunting, or slowing of crack propagation, increases the loading time which allowed the force to continue to climb for fixed displacement rate loading conditions before catastrophic interfacial failure proceeds.

One requirement of this mechanism of adhesion enhancement of patterned surfaces is that the interfacial cracks should act discretely, in order to impede propagation and force re-initiation to occur. Patterns act discretely if they are spaced at distances greater than the distance over which adhesives interactions occur, δ_c, defined by[75]:

$$\delta_C \approx \frac{G_C}{E} \tag{4.4}$$

Where E is measured through tensile measurements for a given velocity of loading. From the hemispherical contact adhesion measurements conducted at 5 mm/min, G_c was found to be 0.44 +/-0.07 J/m^2 for the elastomer pads. The elastic modulus of the bulk x-PDMS elastomer was measured to be ~1.7 MPa from uniaxial tensile measurements. Substituting these values in to equation 4, we found the critical length scale was approximately 260 nm. This length was less than the spacing (*s*) of the patterned features, suggesting that the lines acted discretely. Furthermore, as δ_c was greater than

the depth of the patterned features, once troughs create contact with the glass, they should not spontaneously separate, which is consistent with our observations. At these testing velocities, these patterns acted discretely, but made equivalent contact area to a non-patterned substrate. The material properties of x-PDMS and geometric dimensions of the patterns gave some insight into the enhanced adhesion mechanism.

The results for 5 mm/min prompted the examination of the interface during testing. In figure 4.8, we show crack propagation images for the non-patterned sample and the two CD line configurations.

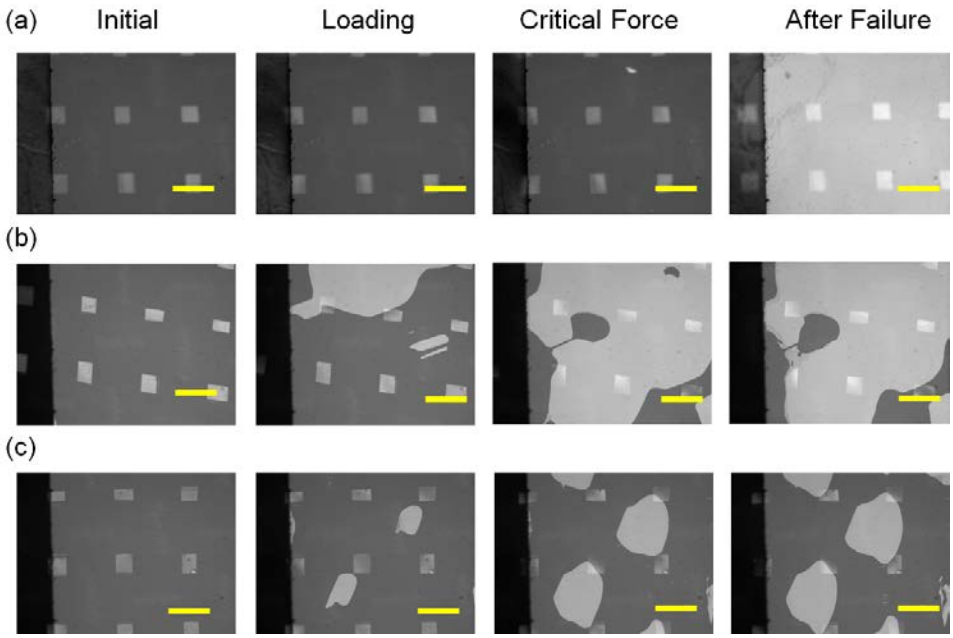

Figure 4.8: Optical micrographs of shear testing. Optical micrograph images of shear testing for the non-patterned fabric composite (a), CD parallel configuration (b), and CD orthogonal configuration (c). The left column is the initial state of all three samples, the second column is an image of the sample while loading, the third column is the sample at the critical force for each configuration and finally the right column is the sample after failure has occurred at the interface. The open squares are gaps in the fabric between adjacent fiber bundles. The scale bars are all 1 mm. Figure reproduced from Pendergraph *et al.*[124]

In the non-patterned sample, the entire area was maintained until the critical force was reached and then the entire interface failed instantaneously. The crack propagation occurred in the direction parallel to the testing direction. In the parallel configuration, there was partial separation of the interface, where the separation grew anisotropically along the direction of the lines. The interface then failed, followed by sliding of the elastomeric interface. Lines oriented parallel to the crack propagation direction did not alter, or slow, the unstable adhesive failure. Furthermore, similar to the results of Chung and Chaudhury, we observed no increased interfacial critical pull off stress for the lines oriented parallel to the crack propagation direction[14]. In the orthogonal configuration, we again saw anisotropic, partial separation of the interface while the sample was being loaded. After the critical force was reached, the sample began to slide similar to the parallel example. Although some separation occurs in the direction of propagation, the lines generally diverted the crack growth. This crack blunting mechanism allowed the adhesive to remain in contact for a longer duration during loading at fixed displacement rates, and thus the orientation gave rise to larger adhesive stress capacities.

4.3.3 Velocity Dependence on Critical Force

To further explore the crack blunting mechanism the testing velocity dependence for these systems was investigated. In figure 4.9, four different testing velocities were implemented and the corresponding adhesive stress capacities are shown.

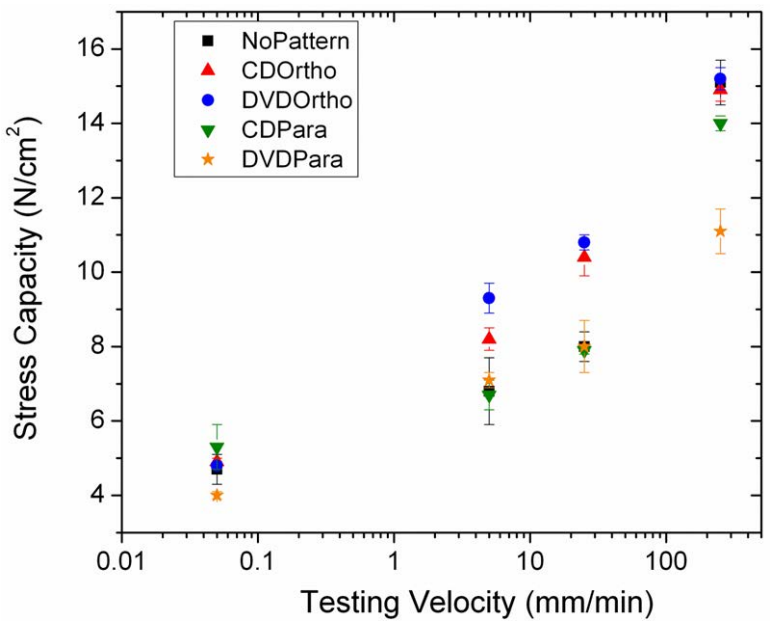

Figure 4.9: Plot of stress capacity vs. test velocity. Adhesive Stress capacity of the samples versus testing velocity over four different testing velocities (0.05, 5, 25 and 250 mm/min). Each point represents the average adhesive stress capacity over 5 tests with the error bars representing the scatter. Adhesion enhancement for the two orthogonal configurations can be seen in 5 mm/min and 25 mm/min; however, nearly all adhesive pads produce equivalent adhesive stress capacities, within error, at the two extreme testing velocities of 0.05 mm/min and 250 mm/min. Figure reproduced from Pendergraph *et al.*[124]

In the intermediate velocity region (5 and 25mm/min) we observed adhesion enhancement for the orthogonal configuration in both the DVD and CD line patterns. At these velocities, the elastomeric interface appeared to be affected by the pattern orientation. The contact area was maintained for longer loading time intervals and thus the load in the sample can be increased for the patterned substrates. For the lowest velocity, we believe that the enhancement was not observed because the crack velocity was moving at a much greater rate than the loading of the sample. Therefore, the interface failed before the load can increase, thus higher pull off forces were not observed. In the highest testing velocity, the adhesion enhancement disappeared because the crack propagation was driven by the testing velocity. The instrument velocity was

likely faster than the crack propagation velocity. Given a constant contact area, all samples were given equal time to load and thus have approximately the same adhesive stress capacity. Furthermore, since G_c has been shown to increase as a function of velocity[75], it is possible that the increase in G_c would cause the line discontinuities to no longer be discrete. Coupling of the features would render them ineffective in crack blunting. It is important to note that despite the lack of differentiating behavior in the patterned substrates, a maximum F_c was achieved at 250 mm/min.

From our previous work on the adhesion of elastomeric fabric composites, the improvements with these composites should be scalable to larger adhesive pad sizes, as long as the (a/D) ratio is sufficiently small. Alternatively, several adhesives of smaller areas can be coupled to create a single pad of larger area.[47] The advantage of this strategy is potentially attenuating the demand for creating a large area pattern, which would increase the probability of defects. The combination of the elastomeric fabric composites allows low cost and facile patterning on the testing surface as well as flexibility in terms of the geometry that can be used to create robust, reversible adhesives.

4.4 Conclusions

In summary, we have evaluated the shear adhesion of patterned elastomeric fabric composites. We implemented a simple fabrication procedure that utilized line features, similar to patterns found in nature. The orientation of the patterning proved to be critical where a line arrangement orthogonal to the testing direction is essential for adhesion enhancement. At intermediate velocities, adhesion enhancement of up to 37% was observed with orthogonally patterned lines compared to adhesive values from equivalent

non-patterned fabric composites. Furthermore, we demonstrated how adhesion enhancement was a function of the fixed displacement rate, the pattern geometry and orientation, and the elastomer materials properties. In particular, the crack blunting mechanism allowed the composite adhesive to remain in contact longer when the displacement rate was greater than but near the slowed debonding crack velocity of the adhesive pad, resulting in adhesion enhancement by allowing the force to climb at intermediate testing velocities. These results will guide the design of patterned adhesives to create robust and reversible adhesives.

CHAPTER 5

CONCLUSIONS

The work described in this thesis encompasses new strategies for patterning fibrous materials. These studies provide the capability to enable a tunable and systematic approach to modify the topography of curved structures that previously was not studied. Individual fibers and larger fabric assemblies can be modified with adjustable parameters such as material selection, pattern sizes, and geometric arrangements. The possible applications that are enabled from these advances will be the impetus for the continuation of this research beyond this thesis.

Since fibers are ubiquitous in many industries and applications, we were motivated to look at the limits of patterning on fibrous structures and sought to improve upon the current technology. Furthermore, it was also important to work with a fibrous material that has technological relevance for many applications. Through this motivation, we chose to work with carbon fiber. Carbon fiber allowed us to pursue new patterning limits in terms of the size of the fiber diameter, yet work with a material that is used in many applications, such as robust structural composites and electrical devices.

A novel colloidal patterning technique was first applied to carbon fibers where a free-standing, assembled array of colloids is transferred to fibers while supported by an underlying substrate. The important aspect of this transfer technique is that a thin layer of water keeps the colloidal crystals planar and intact. As the water is evaporated, the array conforms to the curved surface of the fiber and maintains the order of the array. This method can be applied to a number of fibers on different supporting substrates. Transferring the colloidal arrays in this manner permits a large number of fibers to be

patterned simultaneously over relatively large areas (> 1cm). Carbon fibers possess the ability to be conductive as well as mechanically robust; Patterns can be used in the future for the assembly of functional devices on the surface of the carbon fiber. Knowing that the colloidal patterned fibers can be used as a template for subsequent material deposition, high surface area patterns can be formed on the fiber circumference. The electrochemistry on the carbon fiber also provides a general platform for this patterning to be applied to other conductive fibers, such as metal wires. The formation of submicrometer sized patterns highlights a new potential for nanotechnology on non-planar materials as well as the formation of hierarchical architectures.

In addition to the fabricating submicrometer features on individual fibers, fabric assemblies were also patterned. Inspired by previous work on soft elastomer composites with fabrics, a better understanding of the mechanical properties of these materials was accomplished. The use of a soft, elastic resin in a composite with carbon fiber fabrics gave unique mechanical properties not found in other flexible substrates. Specifically, high in-plane mechanical resistance was observed with retention of bending flexibility. These characteristics are not limited to the resin and fabric materials that were used in the mechanical testing and can be tuned for constraints in material properties or applications. Since, soft and conformable resins were used, patterning of these composites was then studied. These patterns can be formed on the surface of the resin and are stable to rapid deformation of the composite. This has enabled the topography of the composite structure to be tuned. The capabilities to adjust the fabric, resin and the patterning on the surface enable a copious number of potential applications, such as flexible electronics and biomedical devices.

One application has been shown in the final section of the thesis, which pertains to the shear adhesion of the fabric composites. The patterning procedure described in the section before enabled the ability to modify the topography of the surface. Through the examination of an array of patterned lines, the orientation and spacing of these lines were observed to modify the composites adhesion to surfaces. Improved adhesion was observed at certain velocities, yet at very low and high testing velocities, the patterns were typically comparable to a non-patterned material. These patterned composites may have implications on adhesion, especially in dynamic systems such as climbing where this patterning may allow higher loads to be achieved.

APPENDIX

Mechanical Properties of Elastomeric Fabric Composites

A.1 Introduction

In chapter 3, elastomeric composites were shown to possess unique mechanical properties not possible in homogenous materials. Fiber composites have been well known to combine characteristics of one material with another one, allowing for unique attributes to be achieved.[72, 125] Many examples of this include taking a polymeric resin and then combining it with inorganic or carbon filler to increase the tensile strength and fracture resistance. In recent studies, a novel concept of implementing a soft resin with a rigid fabric has enabled unprecedented strengths for a reversible adhesive.[30, 47] In these examples, a soft elastomer allowed for intimate contact against smooth surfaces. When the resin was held sufficiently thin and the composite is loaded in shear, the load is subsequently transferred to the rigid fabric. The fabric was loaded in tension, which is the direction of highest stiffness. Conversely, when the composite was peeled off the surface, the combination of the fabric and the fiber geometry in bending facilitates the adhesive peeling off easily due to the significantly lower stiffness.

The use of flexible substrates for applications such as electronics requires the knowledge of many characteristics.[87] In chapter 3, some of the mechanical properties were evaluated, primarily the moduli of the materials. However, knowing how a material will fail or the critical limits to its mechanical integrity are also imperative to product design. In this chapter, we will continue the discussion of the mechanical properties to include the ultimate tensile strength and the strain limits in uniaxial tensile testing. The

differences in the failure mechanism are described. The energy required for bending the samples are calculated. From the bending tests, the different causes for hysteresis in the loading and the unloading sections of the bending test are discussed.

A.2 Experimental

A.2.1 Fabrication of Composites

The fabrication of the composites was produced in the same method as in chapters 3 and 4.[106, 124] Briefly, a filling substrate (e.g. paper, carbon fiber fabric) was placed onto a sheet of poly(ethylene terephthalate) (PET). Next, degassed Sylgard 184 (10:1 ratio of prepolymer to curing agent) was added on top of the sample and allowed to diffuse into the sample. A blank Digital Video Disk (DVD) mold was then placed on top of the sample followed by a second PET sheet. The samples were allowed to cure at room temperature for 3 days and then subsequently cured at for 1 hour at 70^{o} C. The molds were removed and then samples were cut into 1.2 cm wide x 4 cm long for bending samples. The tensile samples were cut using a dogbone mold with the span length of 2.6 cm long and an interior width of 0.46 cm wide.

A.2.2 Mechanical Testing of Composites

Tensile testing was run at 1 mm/min with an Instron 5500R, similar to literature procedures.[106]

A.2.3 Bending Testing of Composites

Bending testing was conducted by implementing a 3-point bending test with a vertical displacement of 1 mm at a rate of 1 mm/min and a constant span length of 1.92 cm.[106]

A.3 Results and Discussion

A.3.1 Tensile Testing of Composites

The materials were selected to be tested to evaluate the differences in their mechanical behavior. First, uniaxial testing was performed at a rate of 1 mm/min. A compilation of tensile curves are compiled for all seven types of samples in figure A.1.

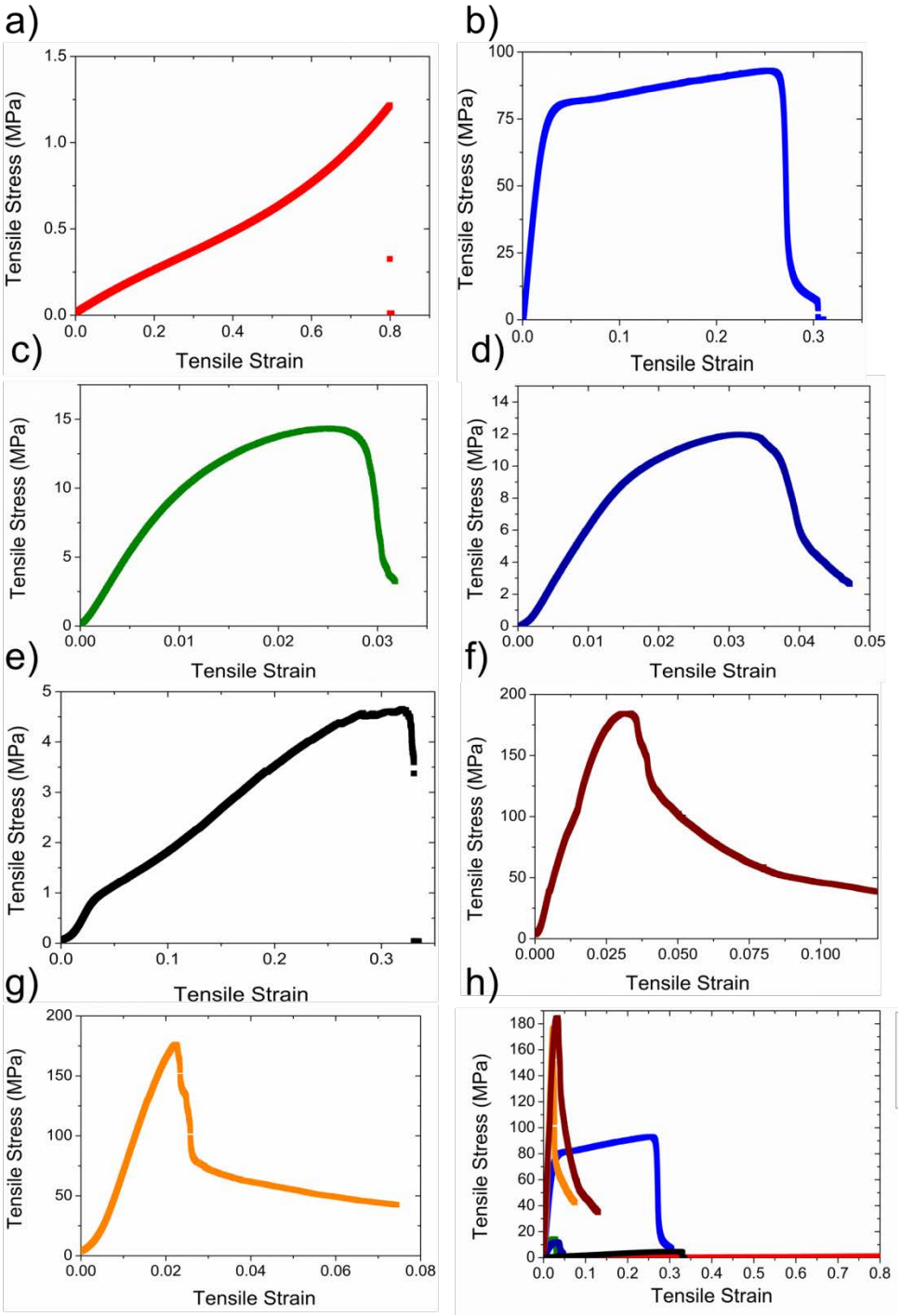

Figure A.1: Compilation of the tensile curves. Stress vs. Strain for: x-PDMS (a), PET (b), Cellulose (c), Cellulose/x-PDMS (d), transverse (1-D ortho)/x-PDMS (e), axial (1-D para)/x-PDMS (f), plain weave (2-D)/x-PDMS (g) and a summary plot (h).

In all of the samples, uniaxial strain was applied until a maximum stress was obtained and followed by the failure of the material. This critical stress was defined as the ultimate tensile strength. The strain of the material was characterized by the following equation:

$$\varepsilon_T = \frac{\Delta L}{L_o} \quad \text{(A.1)}$$

Where ε_T is the tensile strain, ΔL is the change in length of the sample and L_o is the original length of the material.

In order to understand the effect that the elastomer has on the components, we first evaluated the Sylgard 184 material (referred to from now on as x-PDMS). Out of all of the materials, it possessed the lowest ultimate tensile strength (1.00 ± 0.35 MPa), which was commensurate with its low modulus from chapter 3.[106] Conversely, this material also possessed the highest strain at the ultimate tensile strength (0.74 ± 0.20), which was comparable to previously reported values for this elastomer.[55, 92, 93] The x-PDMS failed suddenly at the maximum tensile stress of the material. Another homogenous material that was tested was filter paper (cellulose). Filter paper was composed of non-oriented fibers; therefore by testing cellulose, a fiber based sample can be examined with no preferential axial direction. Cellulose was stiffer with an ultimate tensile strength of 16.3 ± 0.9 MPa and a significantly lower corresponding strain of 0.024 ± 0.004, than x-PDMS. The samples failed precipitously, but not instantaneously like x-PDMS after the ultimate tensile stress was obtained due to the fibrous structure of the material that prevents sudden catastrophic failure. The third homogeneous material that was tested was polyethylene terephthalate (PET), a rigid semi-crystalline polymer. The ultimate tensile

stress was substantially higher at 98.8 ± 9.9 MPa and a strain of 0.23 ± 0.02. The stress profile of the material was also different than the other materials. After the initial linear elastic region, the slope changed and the polymer began to plastically deform (strain harden), which was caused by crystallization of the polymers.[72] The stiffness of the system decreases, however the material continues to increase in tensile stress. After the ultimate tensile force was reached, the material failed precipitously, however not instantaneously. The remaining samples, the combination of the x-PDMS and the reinforcing material (i.e. paper or carbon fiber) created a hybrid material between the Sylgard 184 and the other material.

The other materials in figure A.1 were composites with different fiber orientations. x-PDMS was the resin for all of the composites with carbon fiber for the uni-directional axial, uni-directional and two dimensional ordered fibrous networks. For the cellulose/x-PDMS composite, the ultimate tensile stress decreased 17% to 13.9 ± 2.1 MPa; however the strain at the ultimate stress increased to 0.030 ± 0.001. The decrease in ultimate stress was expected because a lower modulus material was incorporated into the composite. The two components were in an isostrain state, where displacement in the material occurred when the strongest component was strained.[72] The strain at the ultimate tensile stress increased by 20%, which was due to two factors: the soft elastomer matrix allowing work to dissipate force as well as the ability for the matrix to adjacent fibers more effectively.[126]

The carbon fiber fabrics were subsequently tested to examine the effect of the orientation of the reinforcing component on the composite strength. First, fibers oriented axially exhibited a high tensile strength of 129.3 ± 50.8 MPa and a low tensile strain of 0.033 ±

0.007. This was expected due to the high modulus and strength of carbon fibers. Similarly, the plain weave carbon fiber fabric also displayed a higher tensile strength of 163.9 ± 25.7 MPa and a tensile strain of 0.026 ± 0.003. Similar to the cellulose/x-PDMS, the axially oriented (1-D para) and the plain weave fabrics (2-D), had fibers run continuously through the length of the material. These composites were also in an isostrain condition.[72] Another attribute of the failure was that the failure did not occur instantaneously or precipitously. There was a continuous decrease in the mechanical load, which was caused due to fibers breaking and conversely being pulled out of the matrix.[72, 125] In the transverse material, the tensile strength decreased significantly to 6.17 ± 2.61 MPa and a strain at the ultimate tensile strength of 0.31 ± 0.01. Unlike the prior two carbon fiber composites, there were no continuous fibers running parallel to the straining direction. This configuration placed the components in an isostress condition, where all components were subjected to the same stress.[72] Since the matrix was significantly weaker than the fiber, the ultimate tensile strength was reduced from the other fiber composites.[72] While the ultimate tensile stress and modulus were larger than pure x-PDMS, the mechanical properties were predominated by the matrix. The strain at the ultimate tensile strength was increased by an order of magnitude compared to the other carbon fiber composites. Since the components were subjected to similar stresses, the matrix was allowed to strain rather than having the stress being transferred to the fibers.

A.3.2 Bending Testing of Composites

All of the samples were tested in flexure at a displacement rate of 1 mm-min and a span length of 1.92 cm. The samples were all bent to a vertical displacement of 1 mm, which

corresponded to a radius of curvature (R) of 0.046 and then the deflection was unloaded at the same velocity, shown in figure A.2.

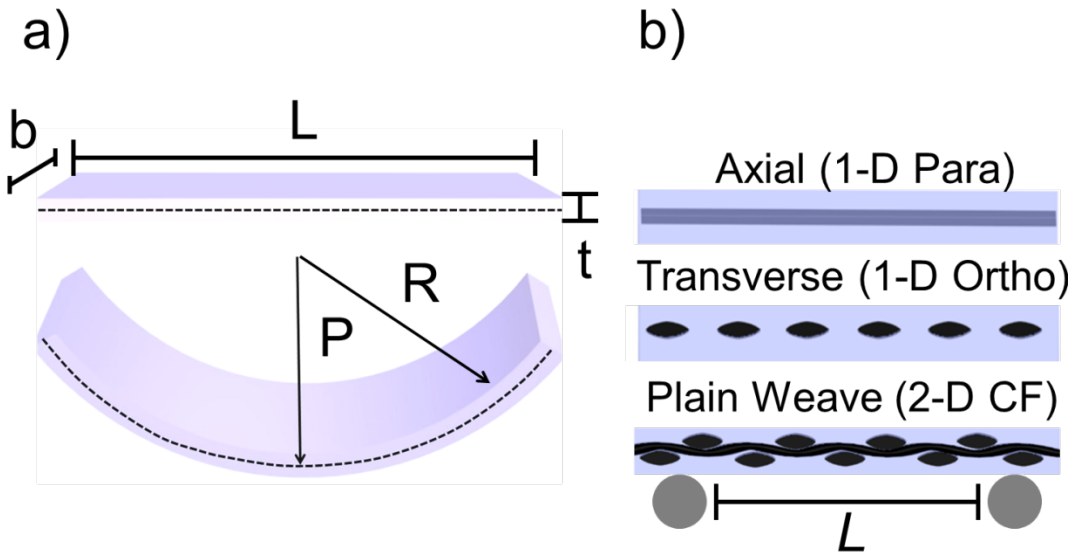

Figure A.2: General bending schematic. a) Geometric representation of the bending and the sample in flexure; b) Side perspective of three carbon fiber composites.

A compilation of force vs. displacement curves are shown in figure A.3.

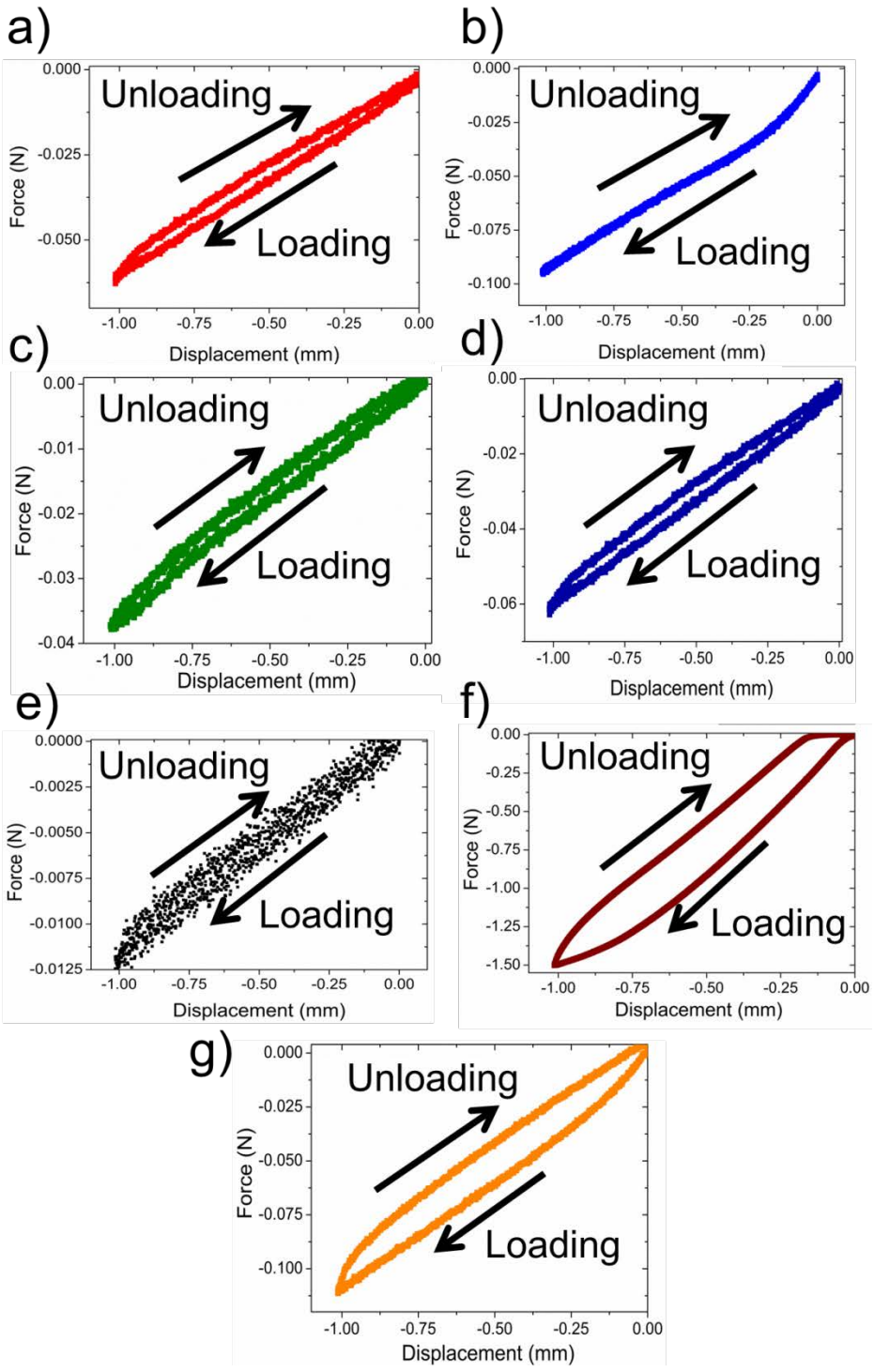

Figure A.3: **Compilation of the bending curves. Force vs. displacement for: x-PDMS (a), PET (b), Cellulose (c), Cellulose/x-PDMS (d), transverse (1-D ortho)/x-PDMS (e), axial (1-D para)/x-PDMS (f), plain weave (2-D)/x-PDMS.**

From knowing the radius of curvature, the maximum bending strain (ε_B) of the individual samples was calculated from equation A.2:

$$\varepsilon_B = \frac{t}{2R} \tag{A.2}$$

Where *t* is the thickness of the sample. The average maximum strains ranged between 0.141% (PET) and 2.7% (PDMS), respectively. All of the samples were strained within the elastic limit relative to their corresponding tensile tests. The bending energy for the composites was calculated by an integration of the force vs. displacement curve from equation A.3:

$$U_B = \int P d\delta \tag{A.3}$$

Where U_B was the bending energy of the system, P was the load applied to the flexure and δ is the vertical displacement. In figure A.5, the average bending energy, taken from the loading segment of the cycle, was normalized by the sample volume:

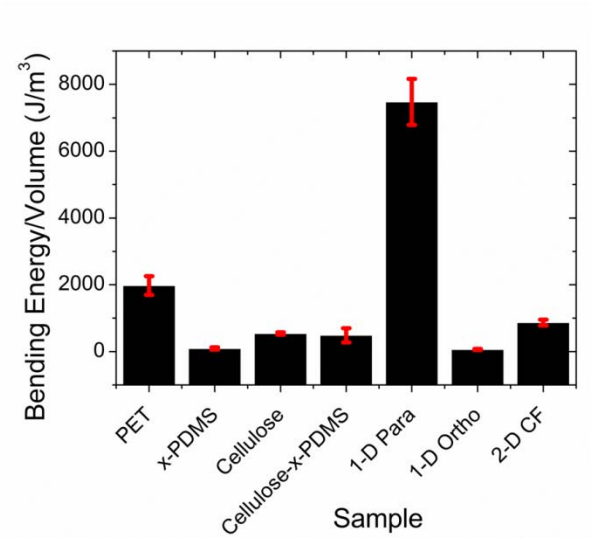

Figure A.4: Compilation of the bending energy per unit volume.

In chapter 3, the bending moduli were evaluated by using the stiffness measurement of the loading section and applying this to equation 3.2. PET had the largest bending modulus of 6.8 GPa, however had the second highest bending energy/volume at 1975 ± 240 J/m^3. The transverse sample (1-D ortho) had the smallest bending energy/volume 60.3 ± 16.9 J/m^3. This value was comparable to x-PDMS at 91.6 ± 35.6 J/m^3 and corresponded to the two samples being the two most compliant that were tested. Cellulose and x-PDMS/cellulose had comparable values to each other, with 539 ± 34.3 J/m^3 and 486 ± 212 J/m^3, which was expected due to their similar bending modulus values. The plain weave (2-D)/x-PDMS composite required 866 ± 86.7 J/m^3, which was lower than 1-D para/x-PDMS and the PET samples. Similar to the bending modulus, the lower energy required was due to weave structure that facilitates bending in the composite.[106, 108] Interestingly, the 1-D para/x-PDMS had the highest energy/volume 7478 ± 648 J/m^3. Although the bending modulus of this sample was lower than PET, the

high energy/volume ratio at this sample geometry shows that the majority of the load was transferred to the carbon fibers, similar to the tensile testing.

In an elastic system, there should be no difference between the pathway in the loading and unloading segment in the bending test. However, discrepancies between the two curves give rise to energy loss in the system known as hysteresis. In all samples, there was hysteresis observed between the samples. PET had the least amount of hysteresis. x-PDMS displayed hysteresis, which was due to viscoelastic effects in the material. Cellulose had some hysteresis in the sample, which was due to deformation and frictional forces between the fibers. All composites also displayed hysteresis between the loading and unloading phases of the test. Cellulose/x-PDMS composite had slightly more energy lost than the pure cellulose, due to the combination of friction between the fibers and the matrix separating from the fibers.[126] The transverse carbon fiber composite had little hysteresis, due to the matrix stretching rather than the fibers moving during flexure. A schematic of the differences between the fiber orientations of the carbon fiber fabrics is shown in figure A.1b. The axially and plain weave oriented fiber composites had larger hysteresis compared to the other samples. In both of these cases, similar to the tensile testing, the load was transferred through the fiber throughout the entire composite, thus increasing the bending stiffness of the material. The mechanical properties of the samples were reversible between cycles (i.e. the loading stiffness was recoverable). One source of the hysteresis was analogous to carbon black filled rubber, where fracture between the matrix and the carbon black led to hysteresis in samples.[127] Similar to our tests, the rubber samples recovered the adhesion between the rubber and the carbon black when the

sample became unstrained. Other mechanism of hysteresis can arise from friction between fabrics and the resin.[128]

A.4 Conclusions

In this section we described some of the mechanical properties of the materials used in creating flexible, patterned substrates. The ultimate tensile stress and corresponding strain were reported for all of the samples as well as discussion on the different failure mechanisms that occurred within the samples. Samples were also subjected to a reversible, cyclic bending test. The materials were strained to a constant radius of curvature and the energy per unit volume was calculated. Most of the samples corresponded with the modulus trends in chapter 3. However the axial fiber composite had a considerably higher energy per volume than the highest bending modulus material PET. Finally, the hysteresis mechanisms for the composites were discussed. Through the knowledge in this chapter, these characteristics can help further guide the design of substrates for flexible material applications.

REFERENCES

[1] L. Feng, S. H. Li, Y. S. Li, H. J. Li, L. J. Zhang, J. Zhai, Y. L. Song, B. Q. Liu, L. Jiang, D. B. Zhu, *Adv. Mater.* **2002**, *14*, 1857.

[2] T. L. Sun, L. Feng, X. F. Gao, L. Jiang, *Accounts Chem. Res.* **2005**, *38*, 644.

[3] J. Y. Chung, M. K. Chaudhury, *J. R. Soc. Interface* **2005**, *2*, 55.

[4] E. P. Chan, D. Ahn, A. J. Crosby, *J. Adhes.* **2007**, *83*, 473.

[5] C. Greiner, A. del Campo, E. Arzt, *Langmuir* **2007**, *23*, 3495.

[6] M. P. Murphy, B. Aksak, M. Sitti, *J. Adhes. Sci. Technol.* **2007**, *21*, 1281.

[7] A. Jagota, C. Y. Hui, N. J. Glassmaker, T. Tang, *MRS Bull.* **2007**, *32*, 492.

[8] S. N. Gorb, *Philos. Trans. R. Soc. A-Math. Phys. Eng. Sci.* **2008**, *366*, 1557.

[9] L. Shen, N. J. Glassmaker, A. Jagota, C. Y. Hui, *Soft Matter* **2008**, *4*, 618.

[10] A. Kumar, H. A. Biebuyck, G. M. Whitesides, *Langmuir* **1994**, *10*, 1498.

[11] S. Y. Chou, *Proc. IEEE* **1997**, *85*, 652.

[12] H. Sirringhaus, T. Kawase, R. H. Friend, T. Shimoda, M. Inbasekaran, W. Wu, E. P. Woo, *Science* **2000**, *290*, 2123.

[13] J. A. Rogers, Z. Bao, K. Baldwin, A. Dodabalapur, B. Crone, V. R. Raju, V. Kuck, H. Katz, K. Amundson, J. Ewing, P. Drzaic, *Proc. Natl. Acad. Sci. U. S. A.* **2001**, *98*, 4835.

[14] B. Michel, A. Bernard, A. Bietsch, E. Delamarche, M. Geissler, D. Juncker, H. Kind, J. P. Renault, H. Rothuizen, H. Schmid, P. Schmidt-Winkel, R. Stutz, H. Wolf, *IBM J. Res. Dev.* **2001**, *45*, 697.

[15] Y. L. Loo, R. L. Willett, K. W. Baldwin, J. A. Rogers, *Appl. Phys. Lett.* **2002**, *81*, 562.

[16] L. J. Guo, *Adv. Mater.* **2007**, *19*, 495.

[17] A. Mata, A. J. Fleischman, S. Roy, *Biomed. Microdevices* **2005**, *7*, 281.

[18] N. Faisant, J. Siepmann, J. P. Benoit, *Eur. J. Pharm. Sci.* **2002**, *15*, 355.

[19] A. W. Martinez, S. T. Phillips, M. J. Butte, G. M. Whitesides, *Angew. Chem. Int. Ed.* **2007**, *46*, 1318.

[20] N. D. Gallant, J. R. Capadona, A. B. Frazier, D. M. Collard, A. J. Garcia, *Langmuir* **2002**, *18*, 5579.

[21] A. J. Haes, W. P. Hall, L. Chang, W. L. Klein, R. P. Van Duyne, *Nano Lett.* **2004**, *4*, 1029.

[22] J. E. Green, J. W. Choi, A. Boukai, Y. Bunimovich, E. Johnston-Halperin, E. DeIonno, Y. Luo, B. A. Sheriff, K. Xu, Y. S. Shin, H. R. Tseng, J. F. Stoddart, J. R. Heath, *Nature* **2007**, *445*, 414.

[23] S. Wong, V. Kitaev, G. A. Ozin, *J. Am. Chem. Soc.* **2003**, *125*, 15589.

[24] Y. N. Xia, B. Gates, Y. D. Yin, Y. Lu, *Adv.Mater.* **2000**, *12*, 693.

[25] B. R. Ringeisen, J. Callahan, P. K. Wu, A. Pique, B. Spargo, R. A. McGill, M. Bucaro, H. Kim, D. M. Bubb, D. B. Chrisey, *Langmuir* **2001**, *17*, 3472.

[26] F. Greco, A. Zucca, S. Taccola, A. Menciassi, T. Fujie, H. Haniuda, S. Takeoka, P. Dario, V. Mattoli, *Soft Matter* **2011**, *7*, 10642.

[27] F. C. Krebs, *Org. Electron.* **2009**, *10*, 761.

[28] D. H. Kim, Y. S. Kim, J. Wu, Z. J. Liu, J. Z. Song, H. S. Kim, Y. G. Y. Huang, K. C. Hwang, J. A. Rogers, *Adv. Mater.* **2009**, *21*, 3703.

[29] T. Sekitani, T. Someya, *Adv. Mater.* **2010**, *22*, 2228.

[30] M. D. Bartlett, Croll, A. B., King, D. R., Paret, B. M., Irschick, D. J. and Crosby, A. J. , *Adv. Mater., 24* **2012**, *24*, 1078.

[31] P. Jiang, J. F. Bertone, K. S. Hwang, V. L. Colvin, *Chem. Mat.* **1999**, *11*, 2132.

[32] P. Jiang, T. Prasad, M. J. McFarland, V. L. Colvin, *Appl. Phys. Lett.* **2006**, *89*, 011908.

[33] J. C. Hulteen, R. P. Vanduyne, *J. Vac. Sci. Technol. A* **1995**, *13*, 1553.
[34] Y. N. Xia, B. Gates, Y. D. Yin, Y. Lu, *Adv. Mater.* **2000**, *12*, 693.
[35] C. L. Haynes, R. P. Van Duyne, *J. Phys. Chem. B* **2001**, *105*, 5599.
[36] J. Z. Li, P. R. Herman, C. E. Valdivia, V. Kitaev, G. A. Ozin, *Opt. Express* **2005**, *13*, 6454.
[37] X. D. Wang, C. J. Summers, Z. L. Wang, *Nano Lett.* **2004**, *4*, 423.
[38] S. M. Yang, S. G. Jang, D. G. Choi, S. Kim, H. K. Yu, *Small* **2006**, *2*, 458.
[39] C. Li, G. S. Hong, L. M. Qi, *Chem. Mater.* **2010**, *22*, 476.
[40] S. B. Han, A. L. Briseno, X. Y. Shi, D. A. Mah, F. M. Zhou, *J. Phys. Chem. B* **2002**, *106*, 6465.
[41] M. Deutsch, Y. A. Vlasov, D. J. Norris, *Adv. Mater.* **2000**, *12*, 1176.
[42] S. Y. Chou, P. R. Krauss, P. J. Renstrom, *Science* **1996**, *272*, 85.
[43] J. P. Rolland, E. C. Hagberg, G. M. Denison, K. R. Carter, J. M. DeSimone, *Angew. Chem. Int. Ed.* **2004**, *43*, 5796.
[44] T. Bailey, B. J. Choi, M. Colburn, M. Meissl, S. Shaya, J. G. Ekerdt, S. V. Sreenivasan, C. G. Willson, *J. Vac. Sci. Technol. B* **2000**, *18*, 3572.
[45] B. D. Gates, Q. B. Xu, M. Stewart, D. Ryan, C. G. Willson, G. M. Whitesides, *Chem. Rev.* **2005**, *105*, 1171.
[46] E. P. Chan, C. Greiner, E. Arzt, A. J. Crosby, *MRS Bull.* **2007**, *32*, 496.
[47] M. D. Bartlett, Croll, A. B. and Crosby, A. J. , *Adv. Func. Mater.* **2012**.
[48] A. J. Downard, D. J. Garrett, E. S. Q. Tan, *Langmuir* **2006**, *22*, 10739.
[49] F. L. Zhang, T. Nyberg, O. Inganas, *Nano Lett.* **2002**, *2*, 1373.
[50] A. Golzhauser, W. Eck, W. Geyer, V. Stadler, T. Weimann, P. Hinze, M. Grunze, *Adv. Mater.* **2001**, *13*, 806.
[51] P. S. Kelkar, J. Beauvais, E. Lavallee, D. Drouin, M. Cloutier, D. Turcotte, P. Yang, L. K. Mun, R. Legario, Y. Awad, V. Aimez, *J. Vac. Sci. Technol. A* **2004**, *22*, 743.
[52] J. A. Rogers, R. J. Jackman, G. M. Whitesides, *Adv. Mater.* **1997**, *9*, 475.
[53] M. A. Meitl, Z. T. Zhu, V. Kumar, K. J. Lee, X. Feng, Y. Y. Huang, I. Adesida, R. G. Nuzzo, J. A. Rogers, *Nat. Mater.* **2006**, *5*, 33.
[54] M. K. Kwak, C. Pang, H. E. Jeong, H. N. Kim, H. Yoon, H. S. Jung, K. Y. Suh, *Adv. Funct. Mater.* **2011**, *21*, 3606.
[55] J. A. Wu, M. Li, W. Q. Chen, D. H. Kim, Y. S. Kim, Y. G. Huang, K. C. Hwang, Z. Kang, J. A. Rogers, *Acta Mech. Sin.* **2010**, *26*, 881.
[56] E. P. Chan, A. J. Crosby, *Adv. Mater.* **2006**, *18*, 3238.
[57] G. X. Cao, X. Chen, C. R. Li, A. Ji, Z. X. Cao, *Phys. Rev. Lett.* **2008**, *100*, 036102.
[58] S. P. Bhawalkar, J. Qian, M. C. Heiber, L. Jia, *Langmuir* **2010**, *26*, 16662.
[59] J. H. Moon, G. R. Yi, S. M. Yang, *J. Colloid Interf. Sci.* **2005**, *287*, 173.
[60] J. Hong, J. Cho, K. Char, *J. Colloid Interf. Sci.* **2011**, *364*, 112.
[61] M. Muller, M. Karg, A. Fortini, T. Hellweg, A. Fery, *Nanoscale* **2012**, *4*, 2491.
[62] C. W. Yang, J. W. Park, *Surf. Coat. Technol.* **2010**, *204*, 2761.
[63] T. Sekitani, S. Iba, Y. Kato, Y. Noguchi, T. Someya, T. Sakurai, *Appl. Phys. Lett.* **2005**, *87*, 3.
[64] Y. Lu, Y. Zhang, J. A. Lu, A. Mimura, S. Matsumoto, T. Itoh, *J. Micromech. Microeng.* **2010**, *20*, 125013.
[65] H. T. Yan, M. Wang, Y. X. Ge, P. Yu, *Opt. Fiber Technol.* **2009**, *15*, 324.
[66] E. J. Smythe, M. D. Dickey, G. M. Whitesides, F. Capasso, *ACS Nano* **2009**, *3*, 59.
[67] D. J. Lipomi, R. V. Martinez, M. A. Kats, S. H. Kang, P. Kim, J. Aizenberg, F. Capasso, G. M. Whitesides, *Nano Lett.* **2010**, *11*, 632.

[68] H. T. Yan, Z. Q. Zhen, X. Y. Zhao, Z. X. Tang, X. Z. Li, D. F. Han, *Opt. Eng.* **2010**, *49*, 063401.
[69] M. A. Ray, L. Jia, *Adv. Mater.* **2007**, *19*, 2020.
[70] J. Lucassen, *Colloids Surf.* **1992**, *65*, 131.
[71] S. A. Pendergraph, J. Y. Park, N. R. Hendricks, A. J. Crosby, K. R. Carter, *Small* **2013**, *9*, 3037.
[72] I. M. Ward, D.W. Hadley, *An Introduction to the Mechanical Properties of Solid Polymers*, John Wiley & Sons Ltd, Chichester **1993**.
[73] C. A. Schneider, W.S., Rasband, K.W. Eliceiri, *Nat. Methods* **2012**, *9*, 671.
[74] G. Miquelard-Garnier, A. B. Croll, C. S. Davis, A. J. Crosby, *Soft Matter* **2010**, *6*, 5789.
[75] K. R. Shull, *Mater. Sci. Eng. R-Rep.* **2002**, *36*, 1.
[76] K. R. Shull, D. Ahn, W. L. Chen, C. M. Flanigan, A. J. Crosby, *Macromol. Chem. Phys.* **1998**, *199*, 489.
[77] S. Kundu, C. S. Davis, T. Long, R. Sharma, A. J. Crosby, *J. Polym. Sci. Polym. Phys.* **2010**, *49*, 179.
[78] A. S. Sarac, H. Geyik, E. A. Parlak, M. Serantoni, *Prog. Org. Coat.* **2007**, *59*, 28.
[79] A. S. Sarac, G. Sonmez, F. C. Cebeci, *J. Appl. Electrochem.* **2003**, *33*, 295.
[80] J. Y. Yang, D. H. Kim, J. L. Hendricks, M. Leach, R. Northey, D. C. Martin, *Acta Biomater.* **2005**, *1*, 125.
[81] M. R. Abidian, D. H. Kim, D. C. Martin, *Adv. Mater.* **2006**, *18*, 405.
[82] K. Nomura, H. Ohta, A. Takagi, T. Kamiya, M. Hirano, H. Hosono, *Nature* **2004**, *432*, 488.
[83] S. Wagner, S. Bauer, *MRS Bull.* **2012**, *37*, 207.
[84] E. H. Kim, C. W. Yang, J. W. Park, *J. Appl. Phys.* **2012**, *111*, 8.
[85] V. Zardetto, T. M. Brown, A. Reale, A. Di Carlo, *J. Polym. Sci. Polym. Phys.* **2011**, *49*, 638.
[86] K. Alzoubi, M. M. Hamasha, S. S. Lu, B. Sammakia, *J. Disp. Technol.* **2011**, *7*, 593.
[87] W. A. MacDonald, M. K. Looney, D. MacKerron, R. Eveson, R. Adam, K. Hashimoto, K. Rakos, *J. Soc. Inf. Disp.* **2007**, *15*, 1075.
[88] F. C. Krebs, S. A. Gevorgyan, J. Alstrup, *J. Mater. Chem.* **2009**, *19*, 5442.
[89] J. van den Brand, R. Kusters, M. Barink, A. Dietzel, *Microelectron. Eng.* **2010**, *87*, 1861.
[90] M. Melzer, D. Makarov, A. Calvimontes, D. Karnaushenko, S. Baunack, R. Kaltofen, Y. F. Mei, O. G. Schmidt, *Nano Lett.* **2011**, *11*, 2522.
[91] T. Akter, J. Joseph, W. S. Kim, *IEEE Electron Device Lett.* **2012**, *33*, 902.
[92] D. H. Kim, J. H. Ahn, W. M. Choi, H. S. Kim, T. H. Kim, J. Z. Song, Y. G. Y. Huang, Z. J. Liu, C. Lu, J. A. Rogers, *Science* **2008**, *320*, 507.
[93] D. H. Kim, J. Z. Song, W. M. Choi, H. S. Kim, R. H. Kim, Z. J. Liu, Y. Y. Huang, K. C. Hwang, Y. W. Zhang, J. A. Rogers, *Proc. Natl. Acad. Sci. U. S. A.* **2008**, *105*, 18675.
[94] D. H. Kim, N. S. Lu, R. Ghaffari, Y. S. Kim, S. P. Lee, L. Z. Xu, J. A. Wu, R. H. Kim, J. Z. Song, Z. J. Liu, J. Viventi, B. de Graff, B. Elolampi, M. Mansour, M. J. Slepian, S. Hwang, J. D. Moss, S. M. Won, Y. G. Huang, B. Litt, J. A. Rogers, *Nat. Mater.* **2011**, *10*, 316.
[95] I. W. Jung, J. L. Xiao, V. Malyarchuk, C. F. Lu, M. Li, Z. J. Liu, J. Yoon, Y. G. Huang, J. A. Rogers, *Proc. Natl. Acad. Sci. U. S. A.* **2011**, *108*, 1788.
[96] T. Sekitani, U. Zschieschang, H. Klauk, T. Someya, *Nat. Mater.* **2010**, *9*, 1015.
[97] D. H. Kim, N. S. Lu, R. Ma, Y. S. Kim, R. H. Kim, S. D. Wang, J. Wu, S. M. Won, H. Tao, A. Islam, K. J. Yu, T. I. Kim, R. Chowdhury, M. Ying, L. Z. Xu, M. Li, H. J. Chung, H. Keum, M. McCormick, P. Liu, Y. W. Zhang, F. G. Omenetto, Y. G. Huang, T. Coleman, J. A. Rogers, *Science* **2011**, *333*, 838.

[98] A. W. Martinez, S. T. Phillips, G. M. Whitesides, *Proc. Natl. Acad. Sci. U. S. A.* **2008**, *105*, 19606.
[99] A. W. Martinez, S. T. Phillips, B. J. Wiley, M. Gupta, G. M. Whitesides, *Lab Chip* **2008**, *8*, 2146.
[100] A. W. Martinez, S. T. Phillips, E. Carrilho, S. W. Thomas, H. Sindi, G. M. Whitesides, *Anal. Chem.* **2008**, *80*, 3699.
[101] E. Carrilho, S. T. Phillips, S. J. Vella, A. W. Martinez, G. M. Whitesides, *Anal. Chem.* **2009**, *81*, 5990.
[102] R. V. Martinez, C. R. Fish, X. Chen, G. M. Whitesides, *Adv. Funct. Mater.* **2012**, *22*, 1376.
[103] T. Sekitani, Y. Noguchi, K. Hata, T. Fukushima, T. Aida, T. Someya, *Science* **2008**, *321*, 1468.
[104] J. H. Jin, J. H. Ko, S. Yang, B. S. Bae, *Adv. Mater.* **2010**, *22*, 4510.
[105] I. W. Moran, J. R. Ell, K. R. Carter, *Small* **2011**, *7*, 2669.
[106] S. A. Pendergraph, M. D. Bartlett, K. R. Carter, A. J. Crosby, *ACS Appl. Mater. Interfaces* **2012**, *4*, 6640.
[107] F. L. Matthews, Rawling, R.D., *Composite Materials: Engineering and Science*, CRC Press LLC, **1999**.
[108] S. Dejong, R. Postle, *J. Text. Inst.* **1977**, *68*, 350.
[109] M. Khatibzadeh, M. R. Piggott, *Compos. Sci. Technol.* **1996**, *56*, 1435.
[110] S. H. Ahn, L. J. Guo, *ACS Nano* **2009**, *3*, 2304.
[111] D. M. Drotlef, L. Stepien, M. Kappl, W. J. P. Barnes, H. J. Butt, A. del Campo, *Adv. Funct. Mater.* **2013**, *23*, 1137.
[112] A. J. Crosby, M. Hageman, A. Duncan, *Langmuir* **2005**, *21*, 11738.
[113] T. Thomas, A. J. Crosby, *J. Adhes.* **2006**, *82*, 311.
[114] E. P. Chan, E. J. Smith, R. C. Hayward, A. J. Crosby, *Adv. Mater.* **2008**, *20*, 711.
[115] C. Pang, D. Kang, T. I. Kim, K. Y. Suh, *Langmuir* **2012**, *28*, 2181.
[116] H. Shahsavan, B. X. Zhao, *Langmuir* **2011**, *27*, 7732.
[117] S. Vajpayee, K. Khare, S. Yang, C. Y. Hui, A. Jagota, *Adv. Funct. Mater.* **2011**, *21*, 547.
[118] M. P. Murphy, S. Kim, M. Sitti, *ACS Appl. Mater. Interfaces* **2009**, *1*, 849.
[119] J. Lee, B. Bush, R. Maboudian, R. S. Fearing, *Langmuir* **2009**, *25*, 12449.
[120] E. Verneuil, B. Ladoux, A. Buguin, P. Silberzan, *J. Adhes.* **2007**, *83*, 449.
[121] E. Degrandi-Contraires, C. Poulard, F. Restagno, L. Leger, *Faraday Discuss.* **2012**, *156*, 255.
[122] J. Yu, S. Chary, S. Das, J. Tamelier, N. S. Pesika, K. L. Turner, J. N. Israelachvili, *Adv. Funct. Mater.* **2011**, *21*, 3010.
[123] D. R. Paretkar, M. D. Bartlett, R. McMeeking, A. J. Crosby, E. Arzt, *J. Adhes.* **2013**, *89*, 140.
[124] S. A. Pendergraph, M. D. Bartlett, K. R. Carter, A. J. Crosby, *ACS Appl. Mater. Interfaces* **2014**, *6*, 6845.
[125] J. Hutchinson, H. Jensen, *Mech. Mater.* **1990**, *9*, 139.
[126] A. Marais, S. Utsel, E. Gustafsson, L. Wågberg, *Carbohyd. Polym.* **2014**, *100*, 218.
[127] A. R. Payne, R. E. Whittaker, *Rubber Chem. Technol.* **1971**, *44*, 440.
[128] W. Van Paepegem, K. De Geyter, P. Vanhooymissen, J. Degrieck, *Compos. Struct.* **2006**, *72*, 212.